TECHNICAL REPORT BRL-TR-3074

BRL

SIDE MOMENT EXERTED BY A SPINNING, CONING, HIGHLY VISCOUS LIQUID PAYLOAD

CHARLES H. MURPHY
JAMES W. BRADLEY
WILLIAM H. MERMAGEN, SR.

DECEMBER 1989

U.S. ARMY LABORATORY COMMAND

BALLISTIC RESEARCH LABORATORY
ABERDEEN PROVING GROUND, MARYLAND

DESTRUCTION NOTICE

Destroy this report when it is no longer needed. DO NOT return it to the originator.

Additional copies of this report may be obtained from the National Technical Information Service, U.S. Department of Commerce, Springfield, VA 22161.

The findings of this report are not to be construed as an official Department of the Army position, unless so designated by other authorized documents.

The use of trade names or manufacturers' names in this report does not constitute indorsement of any commerical product.

REPORT DOCUMENTATION PAGE

Form Approved
OMB No. 0704-0188

1a. REPORT SECURITY CLASSIFICATION UNCLASSIFIED	1b. RESTRICTIVE MARKINGS
2a. SECURITY CLASSIFICATION AUTHORITY	3. DISTRIBUTION/AVAILABILITY OF REPORT Approved for public release; distribution is unlimited
2b. DECLASSIFICATION/DOWNGRADING SCHEDULE	
4. PERFORMING ORGANIZATION REPORT NUMBER(S) BRL-TR-3074	5. MONITORING ORGANIZATION REPORT NUMBER(S)
6a. NAME OF PERFORMING ORGANIZATION US Army Ballistic Research Laboratory 6b. OFFICE SYMBOL (If applicable) SLCBR-LF	7a. NAME OF MONITORING ORGANIZATION
6c. ADDRESS (City, State, and ZIP Code) Aberdeen Proving Ground, MD 21005-5066	7b. ADDRESS (City, State, and ZIP Code)
8a. NAME OF FUNDING/SPONSORING ORGANIZATION US Army Ballistic Research Laboratory 8b. OFFICE SYMBOL (If applicable) SLCBR-DD-T	9. PROCUREMENT INSTRUMENT IDENTIFICATION NUMBER
8c. ADDRESS (City, State, and ZIP Code) Aberdeen Proving Ground, MD 21005-5066	10. SOURCE OF FUNDING NUMBERS PROGRAM ELEMENT NO. 62618A; PROJECT NO. 1L1 62618AH80; TASK NO.; WORK UNIT ACCESSION NO.
11. TITLE (Include Security Classification) Side Moment Exerted by a Spinning, Coning, Highly Viscous Liquid Payload	
12. PERSONAL AUTHOR(S) Charles H. Murphy, James W. Bradley, and William H. Mermagen, Sr.	
13a. TYPE OF REPORT Technical Report 13b. TIME COVERED FROM _____ TO _____	14. DATE OF REPORT (Year, Month, Day) 15. PAGE COUNT
16. SUPPLEMENTARY NOTATION	

17. COSATI CODES		
FIELD	GROUP	SUB-GROUP
01	01	

18. SUBJECT TERMS (Continue on reverse if necessary and identify by block number)
Liquid Side Moment, Spinning Projectile, Liquid-Filled Cylinder, Coning Projectile, Liquid Payload, Flight Instability

19. ABSTRACT (Continue on reverse if necessary and identify by block number)

Four liquid payload theories--Stewartson (S), Stewartson-Wedemeyer (SW), Kitchens-Gerber-Sedney (KGS), and Hall-Sedney-Gerber (HSG)--are developed within a single unifying framework. Equations are presented that form the basis of interactive computer programs. These programs apply the SW, KGS, and HSG theories not only to their original domain, fully filled cylinders, but to partially filled cylinders, cylinders with a central rod and cylinders containing two liquids. Side moment coefficients from the relatively simple KGS calculations are shown to be a good approximation to results from the more exact HSG theory.

20. DISTRIBUTION/AVAILABILITY OF ABSTRACT ☐ UNCLASSIFIED/UNLIMITED ☒ SAME AS RPT. ☐ DTIC USERS	21. ABSTRACT SECURITY CLASSIFICATION UNCLASSIFIED
22a. NAME OF RESPONSIBLE INDIVIDUAL Charles H. Murphy	22b. TELEPHONE (Include Area Code) 301-278-3109 22c. OFFICE SYMBOL SLCBR-LF

DD Form 1473, JUN 86 Previous editions are obsolete. SECURITY CLASSIFICATION OF THIS PAGE

INTENTIONALLY LEFT BLANK.

Table of Contents

List of Tables

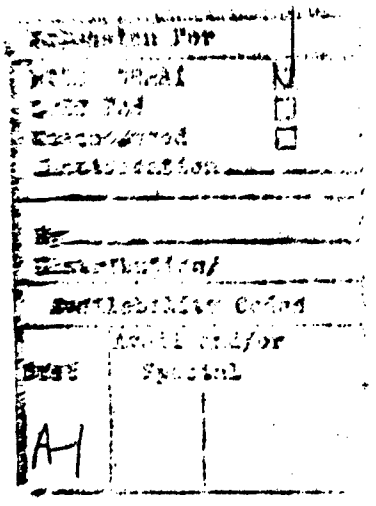

INTENTIONALLY LEFT BLANK.

List of Figures

INTENTIONALLY LEFT BLANK.

I. Introduction

Spinning projectiles containing liquid payloads have shown spectacular instabilities in flight. The first theoretical work by Stewartson[1] in 1959 showed that a spinning inviscid liquid could exert a very large side moment for certain values of τ, the ratio of coning rate to spin rate (symbols are defined in the List of Symbols near the back of this report). In 1965 Wedemeyer[2] added a boundary layer on the container walls; his predicted values of the resonant side moment were verified by experiments using gyroscopes. This Stewartson-Wedemeyer (SW) boundary-layer theory was originally limited to pressure moments, fully- or partially-filled cylindrical cavities, and fully spun-up liquids. Later authors[3–8] extended the theory to include central rods, viscous moments, partially spun-up liquids, two immiscible liquids, and fully-filled spheroidal cavities. In addition, a relation between liquid side moment and liquid roll moment was derived[9] to justify experimental observation of a correlation between these moments.

In 1978 Kitchens, Gerber and Sedney[10] developed a hybrid linear Navier-Stokes theory (hereafter called KGS) that satisfied the boundary conditions on the cylindrical wall exactly by solving a sixth-order system of ordinary differential equations, but it required the addition of boundary layers on the end-walls to satisfy the no-slip condition on these walls. This hybrid high-Reynolds-number theory has been extended to predict the complete moment exerted by both fully spun-up liquids[11,12] and partially spun-up liquids.[13,14]

For very low Reynolds numbers ($Re < 100$), Vaughn et al.[15], Strikwerda et al.[16,17] and Rosenblat et al.[18] have developed Computational Fluid Dynamics (CFD) codes to predict moments for a fully-filled cylinder coning at a constant angle. These predictions showed good agreement with experiments, but this CFD approach requires considerable time on large computing machines. Herbert[19,20] developed an approximate spectral method that requires rather modest computational effort and gives good agreement with the more precise CFD results for $Re < 100$.

Hall, Sedney and Gerber[21] have recently modified the hybrid Navier-Stokes theory to eliminate the approximation of the end-wall boundary conditions. This was done by replacing the simple Stewartson-Wedemeyer spatial eigenvalues by special eigenvalues whose eigenfunctions can be combined to satisfy all the boundary conditions. Once a table of eigenvalues has been constructed, this HSG method can compute liquid moments for $Re < 2500$ on VAX 8600-size computers in less than five minutes. These computations show excellent agreement with the CFD calculations[22] for $Re < 100$ and good agreement with the boundary-layer theories for $Re > 2000$.

The KGS and HSB theories are limited to a fully-filled cylindrical container performing constant-amplitude coning motion. In this report, we will extend these theories to partially-filled cylinders and to cylinders with a central rod. We will also allow the amplitude of the motion to change slowly. Next, we will extend the theories to the case of two immiscible liquids.

In the implementation of the SW, KGS and HSG theories, the liquid moment has usually been computed by integrating the pressure and wall shears over the surface of the cylindrical container. A mathematically equivalent approach is to integrate the angular

momentum over the liquid volume and then differentiate this integral. It will be shown that for the essentially exact HSG theory, the two methods - surface and volume integration - yield the same value for the liquid moment. However, for the less exact SW and KGS theories, the volume integral method gives much 'better' moment values, in the sense that they are in closer agreement with HSG results. Indeed, using the volume integral, the SW theory adequately approximates HSG results down to Re = 500 and KGS adequately approximates HSG down to Re = 1.

II. Equations of Liquid Motion

We will consider a projectile with a cylindrical cavity of radius a and height $2c$ and hence of fineness ratio $A = c/a$. The axis of the cylinder is collinear with the projectile's axis and the cylinder center of mass is located a distance h from the projectile's center of mass. For simplicity, we will assume that $h = 0$; the effect of a nonzero h will be considered in Appendix A.

If the cavity is only partially filled, if the liquid is fully spun-up and if the centrifugal force is large compared to the aerodynamic forces, then in the absence of coning motion the liquid will fill the space between the outer cylindrical wall and an inner cylindrical free surface of radius b. The ratio of the volume of this inner cylinder to the volume of the payload cavity is b^2/a^2. The fill ratio for the payload cavity is thus $1 - b^2/a^2$.

In addition to fully and partially filled cylindrical payload cavities, the case of a cylindrical cavity with a central rod of radius d can be easily treated by the linear theory. The annular region between the inner and outer cylindrical walls will be considered fully filled with liquid.

Although the differential equations of motion are most conveniently expressed in earth-fixed coordinates, the boundary conditions are best expressed in cylindrical coordinates aligned with the projectile's axis of symmetry. Symmetry-axis coordinates have one free parameter: angular velocity about the symmetry axis. If this angular velocity is chosen to be the projectile's spin rate, the system is the usual missile-fixed coordinate system. If this angular velocity is chosen to be zero, we have the nonspinning aeroballistic system used in the flight mechanics of symmetric missiles[23].

Earth-fixed axes X_e, Y_e, Z_e are selected so that X_e is initially along the velocity vector[1] and the X-axis of the missile-aligned system will be along the projectile's axis of symmetry. The angle between the X and X_e axes is the total angle of attack, α_t. The angle between the Z_e-axis and the normal to the plane formed by X and X_e will be called ϕ_α, where $\dot{\phi}_\alpha$ is the precessional rate of the angular motion performed by the projectile about the velocity vector.

Although the angular motion of a projectile does not in general have a constant precessional rate, it can be shown that the linear motion is the sum of two circular motions with constant precessional rates. The objective of all liquid payload theories is to predict

[1] In this report, we assume that the velocity vector maintains a constant direction. The effects of aerodynamic forces and gravity are given in Reference [23].

the liquid moment response to constant-precession angular motion. For these theories, projectile-aligned coordinates that rotate at the precessional rate (coning aeroballistic coordinates) are especially convenient since the boundary conditions are then independent of time.

Let $(\hat{e}_x, \hat{e}_y, \hat{e}_z)$ be unit vectors in the earth-fixed system and let $(\hat{e}_{xc}, \hat{e}_{yc}, \hat{e}_{zc})$ be unit vectors in the coning aeroballistic system. These unit vectors are related as follows:

$$\hat{e}_{xc} = \gamma\hat{e}_x - K(\hat{e}_y \cos\phi_\alpha + \hat{e}_z \sin\phi_\alpha) \quad (1)$$

$$\hat{e}_{yc} = K\hat{e}_x + \gamma(\hat{e}_y \cos\phi_\alpha + \hat{e}_z \sin\phi_\alpha) \quad (2)$$

$$\hat{e}_{zc} = -\hat{e}_y \sin\phi_\alpha + \hat{e}_z \cos\phi_\alpha \quad (3)$$

where

$$K = \sin\alpha_t, \quad \gamma = \cos\alpha_t$$

The angular velocity $\vec{\Omega}$ of the coning aeroballistic coordinate system is defined by the relation

$$(\dot{\hat{e}}_{xc}, \dot{\hat{e}}_{yc}, \dot{\hat{e}}_{zc}) = \vec{\Omega} \times (\hat{e}_{xc}, \hat{e}_{yc}, \hat{e}_{zc}) \quad (4)$$

It can be easily verified that

$$\vec{\Omega} = \tau\dot{\phi}[\hat{e}_x - (\epsilon K/\gamma)\hat{e}_{zc}] \quad (5)$$

$$\hat{e}_x = \gamma\hat{e}_{xc} + K\hat{e}_{yc} \quad (6)$$

where

- $\dot{\phi}$ is the projectile spin rate relative to an inertial frame;
- $\tau = \dot{\phi}_\alpha/\dot{\phi}$, the ratio of the precessional rate to the spin rate; and
- $K = K_0 e^{\epsilon\tau\phi}$. Hence $\epsilon\tau\dot{\phi} = \dot{K}/K$ and we see that ϵ is a measure of the logarithmic damping during a precession cycle. Zero ϵ denotes constant-amplitude coning motion.

Cylindrical coordinates will be denoted by (x, r, θ) in the earth-fixed system and by $(\tilde{x}, \tilde{r}, \tilde{\psi})$ in the coning aeroballistic system. (For convenience, we will assume that all length variables have been made dimensionless by division by the radius a.) From Eqs.(1-3), we have

$$x = \gamma\tilde{x} + \tilde{r}K\cos\tilde{\psi} \quad (7)$$

$$r\cos\theta = \tilde{r}[\cos(\tilde{\psi} + \phi_\alpha) + (\gamma - 1)\cos\tilde{\psi}\cos\phi_\alpha] - \tilde{x}K\cos\phi_\alpha \quad (8)$$

$$r\sin\theta = \tilde{r}[\sin(\tilde{\psi} + \phi_\alpha) + (\gamma - 1)\cos\tilde{\psi}\sin\phi_\alpha] - \tilde{x}K\sin\phi_\alpha \quad (9)$$

For small K, Eqs.(7-9) reduce to

$$x = \tilde{x} + \tilde{r}R\{Ke^{-i\tilde{\psi}}\} \quad (10)$$

$$r = \tilde{r} - \tilde{x}R\{Ke^{-i\tilde{\psi}}\} \quad (11)$$

$$\sin(\tilde{\psi} - \psi) = -(\tilde{x}/\tilde{r})R\{iKe^{-i\tilde{\psi}}\} \quad (12)$$

where

$$\begin{aligned} \psi &= \theta - \phi_a = \theta - \tau\phi \\ \phi &= \dot{\phi}t \\ \phi_a &= \dot{\phi}_a t \end{aligned}$$

and where $R\{\ \}$ denotes the real part of a complex quantity.

The coning cylindrical components of the velocity of a point on the projectile are given by

$$\dot{\tilde{x}} = 0 \tag{13}$$

$$\dot{\tilde{r}} = 0 \tag{14}$$

$$\tilde{r}\dot{\tilde{\psi}} = \tilde{r}\dot{\phi}(1-\tau) \tag{15}$$

The earth-fixed cylindrical components of the velocity can be obtained by differentiating Eqs.(10-12):

$$V_x = a\dot{\phi}R\{i(f-1)rK^*\} \tag{16}$$

$$V_r = -a\dot{\phi}R\{i(f-1)xK^*\} \tag{17}$$

$$V_\theta = a\dot{\phi}[r - R\{(f-1)xK^*\}] \tag{18}$$

where

$$\begin{aligned} K^* &= Ke^{-i\psi} = K_0 e^{i(f\phi-\theta)} \\ f &= (1-i\epsilon)\tau \end{aligned}$$

We will now make the very restrictive assumption that the liquid is in steady-state response to the coning and spinning motion of the projectile. Theoretical studies[5,6] have been made and are in progress to determine the effect of partially spun-up liquid, and an experimental study[24] has been made of the transient response to coning motion. These studies show that spin-up and cone-up effects are large and important to a complete understanding of the liquid-payload stability problem.

Nevertheless, we will assume that the liquid velocity components and liquid pressure have the same dependency on time and θ as do the velocity components of points on the projectile. Accordingly, we introduce three dimensionless complex perturbation velocities: $\underline{w}, \underline{u}, \underline{v}$, each a function of r and x, and write:

$$V_x = -a\dot{\phi}R\{\underline{w}K^*\} \tag{19}$$

$$V_r = -a\dot{\phi}R\{\underline{u}K^*\} \tag{20}$$

$$V_\theta = a\dot{\phi}[r - R\{\underline{v}K^*\}] \tag{21}$$

The equilibrium pressure for a spinning non-coning cylinder is

$$p_{eq} = p_0 + \rho_L a^2 \dot{\phi}^2 \left[\frac{r^2 - r_0^2}{2}\right] \quad (r_0 \le r \le 1) \tag{22}$$

where

- r_0 is either b/a or d/a,
- ρ_L is the liquid density.

When the cylinder is performing coning motion, the outer cylindrical wall is located at $\tilde{r} = 1$. The equivalent earth-fixed radial coordinate of the wall is

$$r_c = 1 - R\{xK^*\} \tag{23}$$

The expression for the earth-fixed radial coordinate of a central rod is similar in form to (23):

$$r_r = r_0 - R\{xK^*\} \tag{24}$$

For a coning, partially filled cylinder, the free surface of the liquid is a slightly perturbed version of a cylindrical surface of radius r_0:

$$r_f = r_0[1 - R\{\underline{\eta}_0(x)K^*\}] \tag{25}$$

To determine $\underline{\eta}_0$, note that the free surface moves with the radial velocity of the liquid at $r = r_0$. Hence differentiation of Eq.(25) yields

$$V_r = -r_0 R\{[i\underline{\eta}_0(x)(af\dot{\phi} - V_\theta/r_0) - \underline{\eta}_0' V_x]K^*\} \tag{26}$$

Thus

$$\underline{\eta}_0(x) = \frac{i\underline{w}(r_0, x)}{(1-f)r_0} \tag{27}$$

The complex liquid pressure perturbation function $\underline{p}$ is, therefore, defined by the relation

$$p = p_0 + \rho_L a^2 \dot{\phi}^2 \left[\frac{r^2 - r_0^2}{2} - R\{\underline{p}K^*\}\right], \quad (r_r, r_f \le r \le r_c) \tag{28}$$

The linearized Navier-Stokes equations for these perturbation functions are

$$\frac{\partial(r\underline{u})}{\partial r} - i\underline{v} + r\frac{\partial \underline{w}}{\partial x} = 0 \tag{29}$$

$$i(f-1)\underline{u} - 2\underline{v} = -\frac{\partial \underline{p}}{\partial r} + \frac{1}{Re}\left[\frac{\partial^2 \underline{v}}{\partial r^2} + \frac{\partial^2 \underline{u}}{\partial x^2} + \frac{1}{r}\frac{\partial \underline{u}}{\partial r} - \frac{2(\underline{u} - i\underline{v})}{r^2}\right] \tag{30}$$

$$i(f-1)\underline{v} + 2\underline{u} = \frac{i\underline{p}}{r} + \frac{1}{Re}\left[\frac{\partial^2 \underline{v}}{\partial r^2} + \frac{\partial^2 \underline{v}}{\partial x^2} + \frac{1}{r}\frac{\partial \underline{v}}{\partial r} - \frac{2i(\underline{u} - i\underline{v})}{r^2}\right] \tag{31}$$

$$i(f-1)\underline{w} = -\frac{\partial \underline{p}}{\partial x} + \frac{1}{Re}\left[\frac{\partial^2 \underline{w}}{\partial r^2} + \frac{\partial^2 \underline{w}}{\partial x^2} + \frac{1}{r}\frac{\partial \underline{w}}{\partial r} - \frac{\underline{w}}{r^2}\right] \tag{32}$$

Each of the four perturbation functions can now be assumed to be the sum of products of two variables: the first a function of r alone and the second a function of x alone:

$$\underline{w} = i(1-f)rH_0(x) - \sum_{k=0}^{N} \hat{w}_k(r)H_k(x) \tag{33}$$

$$\underline{u} = -\left[\frac{i(1-f)^2}{1+f}\right]G_0(x) + \sum_{k=0}^{N} \hat{u}_k(r)G_k(x) \tag{34}$$

$$\underline{v} = -\left[\frac{(1-f)^2}{1+f}\right] G_0(x) + \sum_{k=0}^{N} \hat{v}_k(r) G_k(x) \tag{35}$$

$$\underline{p} = -(1-f)^2 r G_0(x) + \sum_{k=0}^{N} \hat{p}_k(r) G_k(x) \tag{36}$$

In References [4, 10-12],

$$for\ \lambda_0 = 0,\ H_0 = 1\ and\ G_0 = x \tag{37}$$

$$for\ \lambda_k \neq 0,\ H_k = \cos(\lambda_k x)\ and\ G_k = \sin(\lambda_k x) \tag{38}$$

while in HSG, Reference [21],

$$for\ \lambda_0 = 0,\ H_0 = 1\ and\ G_0 = x \tag{39}$$

$$for\ \lambda_k \neq 0,\ H_k = \cos(\lambda_k x)/\sin(\lambda_k A)\ and\ G_k = \sin(\lambda_k x)/\sin(\lambda_k A) \tag{40}$$

The λ_k's are complex parameters arising from this classical separation-of-variables technique and will be evaluated so as to help satisfy the boundary conditions. (The values so determined will be referred to as eigenvalues.) The coefficients of H_0 and G_0 in Eqs.(33-36) are special perturbation functions for $\lambda_0 = 0$. In the low-viscosity theories of References [4, 10-12]:

$$\hat{w}_0 = \hat{u}_0 = \hat{v}_0 = \hat{p}_0 = 0 \tag{41}$$

Eqs.(33-36) can be substituted in Eqs.(29-32) to obtain

$$r\hat{u}_k' + \hat{u}_k - i\hat{v}_k + \lambda_{k1} r \hat{w}_k = 0 \tag{42}$$

$$(Re)^{-1}[\hat{u}_k'' + \hat{u}_k'/r - (B + r^{-2})\hat{u}_k] + 2[1 + i(r^2 Re)^{-1}]\hat{v}_k = \hat{p}_k' \tag{43}$$

$$(Re)^{-1}[\hat{v}_k'' + \hat{v}_k'/r - (B + r^{-2})\hat{v}_k] - 2[1 + i(r^2 Re)^{-1}]\hat{u}_k = -i\hat{p}_k/r \tag{44}$$

$$(Re)^{-1}[\hat{w}_k'' + \hat{w}_k'/r - B\hat{w}_k] = -\lambda_{k2}\hat{p}_k \tag{45}$$

where

$$B = r^{-2} + \lambda_k^2 - i(1-f)Re$$

$$\lambda_{01} = 0$$

$$\lambda_{02} = 1$$

$$\lambda_{k1} = \lambda_{k2} = \lambda_k,\ k \neq 0$$

$$(\ )' = d(\ )/dr$$

These equations can be put in canonical form by the introduction of six new sets of variables Z_{nk} that satisfy the differential equations and a set of constant multipliers c_k that will be used to satisfy the boundary conditions:

$$fc_k Z_{1k}(r) = \hat{u}_k \tag{46}$$

$$fc_k Z_{2k}(r) = \hat{u}_k - i\hat{v}_k \tag{47}$$

$$fc_k Z_{3k}(r) = \hat{v}_k' \tag{48}$$

$$fc_k Z_{4k}(r) = \hat{w}_k \tag{49}$$

$$fc_k Z_{5k}(r) = \hat{w}_k' \tag{50}$$

$$fc_k Z_{6k}(r) = \hat{p}_k \tag{51}$$

For these new variables, Eqs.(42-45) become

$$Z'_{1k} = -Z_{2k}/r - \lambda_{k1} Z_{4k} \quad (52)$$

$$Z'_{2k} = -Z_{2k}/r - \lambda_{k1} Z_{4k} - iZ_{3k} \quad (53)$$

$$Z'_{3k} = 2(Re + ir^{-2})Z_{1k} + i(B + r^{-2})(Z_{2k} - Z_{1k}) - Z_{3k}/r - (iRe/r)Z_{6k} \quad (54)$$

$$Z'_{4k} = Z_{5k} \quad (55)$$

$$Z'_{5k} = BZ_{4k} - Z_{5k}/r - \lambda_{k2} ReZ_{6k} \quad (56)$$

$$Z'_{6k} = (Re)^{-1}[-BZ_{1k} + (2iRe - r^{-2})(Z_{2k} - Z_{1k}) + iZ_{3k}/r - \lambda_{k1} Z_{5k}] \quad (57)$$

III. Boundary Conditions

The boundary condition on each wall of the container is that the liquid must have the same velocity as the wall:

On the cylindrical wall ($\tilde{r} = 1$)

$$\underline{w}(1,x) = i(1-f) \quad (58)$$

$$\underline{u}(1,x) = -i(1-f)x \quad (59)$$

$$\underline{v}(1,x) = -(1-f)x \quad (60)$$

while on the two end-walls ($\tilde{x} = \pm$ A)

$$\underline{w}(r,\pm A) = i(1-f)r \quad (61)$$

$$\underline{u}(r,\pm A) = \mp i(1-f)A \quad (62)$$

$$\underline{v}(r,\pm A) = \mp(1-f)A \quad (63)$$

For a fully-filled container, the conditions on the axis are[10]

$$\underline{w}(0,x) = \underline{u}(0,x) - i\underline{v}(0,x) = \underline{p}(0,x) = 0 \quad (64)$$

On the free boundary of a partially filled container, the tangential shear should vanish and the normal stress should be the inner pressure, p_0.

$$(Re)^{-1}\left[\frac{\partial \underline{v}(r_0,x)}{\partial r} - \frac{i[\underline{u}(r_0,x) - i\underline{v}(r_0,x)]}{r_0}\right] = 0 \quad (65)$$

$$(Re)^{-1}\left[\frac{\partial \underline{w}(r_0,x)}{\partial r} + \frac{\partial \underline{u}(r_0,x)}{\partial x}\right] = 0 \quad (66)$$

$$\underline{p}(r_0,x) + \frac{ir_0\underline{u}(r_0,x)}{1-f} - 2(Re)^{-1}\frac{\partial \underline{u}(r_0,x)}{\partial r} = 0 \quad (67)$$

The no-slip conditions at the rod reduce to:

$$\underline{w}(r_0,x) = i(1-f)r_0 \quad (68)$$

$$\underline{u}(r_0,x) = -i(1-f)x \quad (69)$$

$$\underline{v}(r_0,x) = -(1-f)x \quad (70)$$

IV. Low-Viscosity Solutions

For high Reynolds numbers ($Re > 5000$), three distinct solutions have been obtained to the preceding differential equations and boundary conditions:

1. Stewartson (S) inviscid solution;
2. Stewartson-Wedemeyer (SW) inviscid solution modified by wall boundary layers;
3. Kitchens-Gerber-Sedney (KGS) linear Navier-Stokes solution with end-wall boundary layers.

In all three methods, $c_0 = 0$ and the λ_0 perturbation function for w is $i(1-f)r$, a choice that satisfies the inhomogeneous normal end-wall boundary condition, Eq.(61).

1. Stewartson (S) Solution

For infinite Reynolds number, Eqs.(52-57) reduce to:

$$Z'_{1k} = -Z_{2k}/r - \lambda_k Z_{4k} \tag{71}$$

$$Z'_{6k} = -i(1+f)Z_{1k} + 2iZ_{2k} \tag{72}$$

$$Z_{2k} = -\frac{(1+f)Z_{1k}}{1-f} + \frac{iZ_{6k}}{(1-f)r} \tag{73}$$

$$Z_{4k} = \frac{i\lambda_k Z_{6k}}{1-f} \tag{74}$$

$$Z_{3k} = \left\{\frac{i(1+f)Z_{1k}}{r} + \left[\frac{1}{r^2} - \frac{2\lambda_k^2}{1-f}\right] Z_{6k}\right\}(1-f)^{-1} \tag{75}$$

$$Z_{5k} = \frac{\lambda_k}{(1-f)^2}\left[(3-f)(1+f)Z_{1k} - \frac{2iZ_{6k}}{r}\right] \tag{76}$$

The normal velocity at the flat end-walls, Eq.(61), can be satisfied by

$$c_k = 0, \quad k = 2,4,6,\ldots \tag{77}$$

$$\lambda_k = \frac{k\pi}{2A}, \quad k = 1,2,3,\ldots N \tag{78}$$

Since the perturbation functions vanish for even k, we will take N to be odd and consider only the (N+1)/2 odd k values 1,3,5,...,N both in this section and in the discussions of the SW and KGS solutions that follow. It is interesting to note that the second-order differential equation for Z_{6k} that can be obtained from Eqs.(71-74):

$$r^2 Z''_{6k} + rZ'_{6k} + \left\{\left[\frac{(1+f)(3-f)\lambda_k^2}{(1-f)^2}\right] r^2 - 1\right\} Z_{6k} = 0 \tag{79}$$

is essentially Bessel's equation of order 1. Thus the six Z_{jk}'s are linear combinations of the Bessel functions J_1 and Y_1 and their derivatives; these combinations are given in Table 1.

Next, the normal velocity at the cylindrical wall, Eq.(59), can be satisfied by Eq.(34) when

$$Z_{1k}(1) = 1, \quad c_k = \hat{f} a_k \tag{80}$$

where

$$\hat{f} = \frac{-2i(1-f)}{1+f}$$

and where the a_k's are the coefficients of a least-squares fit of x to a sine series:

$$x = \sum_{k=1}^{N} a_k G_k(x)$$

Since $a_k = 0$ for k even, the c_k's of Eqs.(77) and (80) are compatible.

The second boundary condition for Eqs.(71-74) is

(a) for a fully-filled cylinder:

$$Z_{6k}(0) = 0 \tag{81}$$

(b) for a partially-filled cylinder:

$$Z_{6k}(r_0) + \frac{ir_0 Z_{1k}(r_0)}{1-f} = -\frac{ir_0 f}{2} \tag{82}$$

(c) for a cylinder with a central rod:

$$Z_{1k}(r_0) = 1 \tag{83}$$

2. Stewartson-Wedemeyer (SW) Solution

The Stewartson inviscid solution couldn't satisfy the tangential velocity conditions on the container walls. In 1965 Wedemeyer introduced three oscillatory boundary layers on these walls. These boundary layers created small viscous contributions to the liquid moment, but more importantly they modified the larger inviscid pressure moment term. The boundary layers caused an outflow velocity that changed the normal velocity conditions for the inviscid solution. The presence of the boundary layers on the end walls modifies the eigenvalues, λ_k, and the Fourier coefficients, c_k (see Appendix C). The boundary layer on the lateral, cylindrical wall modifies the boundary condition on $Z_{1k}(1)$ (see Appendix D). Equations (59) and (61) for the inviscid velocity become:

$$u_i(1,x) - \frac{\delta_a e_2}{1-\delta_a e_2} \frac{\partial u_i(1,x)}{\partial r} = -i(1-f)x \tag{84}$$

$$w_i(r,\pm A) - \delta_c \frac{\partial w_i(r,\pm A)}{\partial x} = i(1-f)r \tag{85}$$

where

$$\delta_a = \frac{1+i}{\sqrt{2(1-f)Re}}$$

$$\delta_c = \frac{-(1+i)}{2(1-f)\sqrt{2Re}}\left[\frac{1+f}{\sqrt{3-f}} + \frac{i(3-f)}{\sqrt{1+f}}\right]$$

$$e_2 = \frac{1-e_1^n}{1+e_1^n},\ n=1 \text{ for a central rod; 2 otherwise}$$

$$e_1 = exp[(r_0-1)/\delta_a]$$

For the central rod, a fourth boundary layer modifies Eq.(69):

$$\underline{u}_i(r_0,x) + \left(\frac{r_0\delta_a e_2}{r_0+\delta_a e_2}\right)\frac{\partial \underline{u}_i(r_0,x)}{\partial r} = -i(1-f)x \tag{86}$$

Eqs.(84-86) change Eqs. (78,80,83) to the following:

$$cos(\lambda_k A) + \lambda_k \delta_c\, sin(\lambda_k A) = 0, \quad (k \text{ odd}) \tag{87}$$

$$Z_{1k}(1) - \frac{\delta_a e_2 Z'_{1k}(1)}{1-\delta_a e_2} = 1 \tag{88}$$

$$Z_{1k}(r_0) + \left(\frac{r_0\delta_a e_2}{r_0+\delta_a e_2}\right) Z'_{1k}(r_0) = 1 \tag{89}$$

A good approximate solution of Eq.(87) for the eigenvalues is given by

$$\lambda_k \approx \frac{k\pi}{2(A-\delta_c)} \tag{90}$$

Eq.(90) yields estimates for solving Eq.(87) iteratively for exact values of λ_k. The approximation (90), however, is only valid for $|\delta_c| << A$, in which case the cosine in (87) is nearly zero. For low Reynolds numbers, a solution of Eq.(87) exists for which the cosine has significantly larger magnitude.[25] An adequate first estimate of this special eigenvalue, is given by

$$\lambda_s \approx \pm i/\delta_c \quad for\ |\lambda_s - 1| > 0.1 \tag{91}$$

where the sign is chosen so that the real part of λ_s is positive (usually the minus sign for $\tau < 1$ and the plus sign for $\tau > 1$). This special eigenvalue and its associated eigenfunctions should be included in all summations of the eigenfunctions for boundary conditions and moment coefficients.

The SW solution gives excellent agreement with experiments for $Re > 5,000$.

3. Kitchens-Gerber-Sedney (KGS) Solution

The KGS solution employs the full linearized Navier-Stokes equations [Eqs.(52-57)], but retains the Wedemeyer end-wall boundary layers. This allows the use of the easily computed SW eigenvalues of Eq.(87). The cylindrical boundary layer is eliminated and conditions (58-60) are satisfied exactly. The boundary conditions on the Z_{jk}'s at the outer wall are:

$$Z_{4k}(1) = 0 \tag{92}$$

$$Z_{1k}(1) = 1, \quad c_k = \hat{f} a_k \tag{93}$$
$$Z_{2k}(1) = 0 \tag{94}$$

Note that c_k/a_k is the same as in both the S and SW solutions. The inner boundary conditions are:

(a) for a fully-filled cylinder:[2]

$$Z_{2k}(0) = Z_{4k}(0) = Z_{6k}(0) = 0$$

(b) for a partially-filled cylinder:

$$r_0 Z_{3k}(r_0) - i Z_{2k}(r_0) = 0$$
$$\lambda_k Z_{1k}(r_0) - Z_{5k}(r_0) = \lambda_k$$
$$Z_{6k}(r_0) + \frac{i r_0 Z_{1k}(r_0)}{1-f} - \left(\frac{2}{Re}\right)[i Z_{3k}(r_0) - \lambda_k Z_{4k}(r_0)] = -\frac{i r_0 f}{2}$$

(c) for a cylinder with a central rod:

$$Z_{1k}(r_0) = 1$$
$$Z_{2k}(r_0) = Z_{4k}(r_0) = 0$$

The KGS solution is probably better than the SW solution since it depends on fewer boundary-layer approximations; however, KGS has been limited to applications for which $Re > 1000$. An important characteristic of the KGS method is the fact that it can be modified to give an exact low-Reynolds-number solution (the HSG solution).

V. High-Viscosity (HSG) Solution

In the low viscosity solutions, the k = 0 solution was selected to satisfy the boundary conditions at the flat end-walls. The λ_k's were then the eigenvalues of the differential equations for functions of x. The boundary conditions on the cylindrical wall were then satisfied by a Fourier series fit of these functions.

The HSG method reverses this process. The k = 0 solution is selected to satisfy the boundary conditions on the cylindrical surface. The λ_k's become the eigenvalues of the differential equations for functions of r and the end-wall boundary conditions are satisfied by a least-squares fit to eigenfunctions of r.

The conditions for the k = 0 perturbation functions are:

(a) in general:

$$Z_{10}(1) = 1$$

[2] For computational reasons, conditions are not specified at the singular point $r = 0$ but at some small positive value r_0. The derivatives Z'_{2k}, Z'_{4k} and Z'_{6k} can be obtained from Eqs.(53,55,57) to improve the approximations used. Actually, Reference 10 used a power series in r with as many as thirty terms to relate conditions at $r = 0$ to those at $r = r_0$. If r_0 is taken small enough, one or two terms seem to be sufficient.

$$Z_{20}(1) = Z_{40}(1) = 0$$
$$c_0 = \hat{f}$$

(b) for a fully-filled cylinder:

$$Z_{20}(0) = Z_{40}(0) = Z_{60}(0) = 0$$

(c) for a partially-filled cylinder:

$$r_0 Z_{30}(r_0) - i Z_{20}(r_0) = 0$$
$$Z_{10}(r_0) - Z_{50}(r_0) = 1$$
$$Z_{60}(r_0) + \frac{i r_0 Z_{10}(r_0)}{1-f} - \frac{2i Z_{30}(r_0)}{Re} = -\frac{i r_0 f}{2}$$

(d) for a cylinder with a central rod:

$$Z_{10}(r_0) = 1$$
$$Z_{20}(r_0) = Z_{40}(r_0) = 0$$

The conditions for the $k \neq 0$ perturbation functions are:

(a) in general:

$$Z_{1k}(1) = Z_{2k}(1) = Z_{4k}(1) = 0 \tag{95}$$

(b) for a fully-filled cylinder:

$$Z_{2k}(0) = Z_{4k}(0) = Z_{6k}(0) = 0 \tag{96}$$

(c) for a partially-filled cylinder:

$$r_0 Z_{3k}(r_0) - i Z_{2k}(r_0) = 0 \tag{97}$$
$$\lambda_k Z_{1k}(r_0) - Z_{5k}(r_0) = 0 \tag{98}$$
$$Z_{6k}(r_0) + \frac{i r_0 Z_{1k}(r_0)}{1-f} - \left(\frac{2}{Re}\right)[i Z_{3k}(r_0) - \lambda_k Z_{4k}(r_0)] = 0 \tag{99}$$

(d) for a cylinder with a central rod:

$$Z_{1k}(r_0) = Z_{2k}(r_0) = Z_{4k}(r_0) = 0 \tag{100}$$

For all three inner boundary conditions, the solutions to Eqs.(52-57) must satisfy the homogeneous boundary conditions; hence these solutions are usually identically zero. We can, however, select λ_k so that other solutions are possible. In particular, we will replace the conditions $Z_{1k}(1) = 0$ by $Z_{5k}(1) = 1$ and obtain a set of solutions for particular values of λ_k. This can be done by a numerical orthonormalization process available in a very general and flexible code called SUPORT.[26] This code allows the calculation of $Z_{1k}(1)$ as a function

of λ_k. The value of λ_k that makes $Z_{1k}(1)$ zero is an eigenvalue whose eigenfunctions satisfy all the boundary conditions on the inner and outer cylindrical surfaces, $r = r_0, 1$.

The actual determination of the eigenfunctions is a delicate process. A simple Newton iterative method (strictly speaking, the *regula falsi* method[27]) has been coded; it will converge rapidly to an eigenvalue *if* a good initial guess is available. Hall et al. showed[21] that for a fully-filled cylinder, each eigenvalue falls into one of three families. Figure 1 (from Reference [21]) shows 72 of these eigenvalues for Re = 1000, $\tau = 0.1$. (Note that eigenvalue (3,1) is a maverick in this three-family concept.)

For Re = 10 and $\tau = 0$, the 72 eigenvalues nearest the origin in the half-plane $R\{\lambda_k\} > 0$ were computed by a numerical search process; these 72 eigenvalues are tabulated in Table 2. From these values, additional sets of eigenvalues were generated by taking small steps in both Re and τ. The resulting eigenvalue data base has been stored on our VAX/8600 computer. For the fully-filled cylinder, this base consists of 6216 files, each file containing 72 eigenvalues for a specified pair of values (Re,τ). There are 148 specified Re values:

```
  1  to   20  in steps of   1   [  20 Re values]
 30  to  100  in steps of  10   [   8 Re values]
120  to 2500  in steps of  20   [ 120 Re values]
```

and 42 τ values:

```
 -1  to  -.40  in steps of .10   [   7  values]
-.35  to  -.10  in steps of .05   [   6  values]
  0  to   .10  in steps of .01   [  11  values]
 .15  to   .45  in steps of .05   [   7  values]
 .50  to  1.50  in steps of .10   [  11  values]
```

yielding the 148 x 42 = 6216 files. By interpolating entries in these files, our program obtains good estimates of the 72 eigenvalues when $1 < Re < 2500$ and $-1 < \tau < 1.5$. These starting values allow computation of the 72 eigenvalues in less than five minutes on the VAX.

Similar though not as extensive data bases have been established for the partially-filled cylinder and for the cylinder with a central rod. For both the partially-filled and central-rod cases, files have been created for $1 < Re < 2500$ and $0 < \tau < 0.14$ and for $r_0 = 0.1$ and 0.3. Three-way interpolation (for Re, τ and r_0) then yields good eigenvalue guesses within the specified parameter region.

Once the eigenfunctions are available, they can be used to satisfy the conditions on the end-walls by a proper selection of the c_k's:

$$\sum_{k=1}^{N} c_k Z_{1k}(r) g_k \;=\; R_1 \equiv A\hat{f}[1 - Z_{10}(r)] \qquad (101)$$

$$\sum_{k=1}^{N} c_k Z_{2k}(r) g_k = R_2 \equiv -A\hat{f} Z_{20}(r) \tag{102}$$

$$\sum_{k=1}^{N} c_k Z_{4k}(r) h_k = R_3 \equiv -\hat{f} Z_{40}(r) \tag{103}$$

where

$$g_k = G_k(A)$$
$$h_k = H_k(A)$$

As can be seen from Table 2, the imaginary part of λ_k can be quite large and the use of definition (38) for G_k and H_k would cause g_k and h_k to have extremely large magnitudes. Definition (40) avoids this difficulty.

The c_k's are selected[3] to give the least-squares fit of Eqs.(101-103), where the function to be minimized is

$$R = \int_{r_0}^{1} \{ | \sum c_k Z_{1k} - R_1 |^2 + | \sum c_k Z_{2k} - R_2 |^2 + | \sum c_k Z_{4k} h_k - R_3 |^2 \} r \, dr \tag{104}$$

The quality of the resulting fit is measured by the error e, where

$$e = (R/R_0)^{1/2} \tag{105}$$

and where R_0 is the value of R for $c_k = 0$:

$$R_0 = \int_{r_0}^{1} \{ | R_1 |^2 + | R_2 |^2 + | R_3 |^2 \} r \, dr$$

If $e < .05$, the fit is reasonably good and we have enough eigenfunctions (that is, the value assigned to N is adequate).

VI. Equations for Two Immiscible Liquids

If two immiscible liquids are fully spun-up in a cylindrical container at zero coning angle, they will be separated by a cylindrical interface. At this interface, $r = r_1$, the density and kinematic viscosity will jump from the inner-liquid values (ρ_2, ν_2) to the outer-liquid values (ρ_1, ν_1). The density $\rho_1 = \rho_L$ will be used to nondimensionalize the pressure. The symbol Re will denote the Reynolds number of the outer liquid.

For small-amplitude coning motion, the interface is described by:

$$r_i = r_1[1 - R\{\eta_1(x) K^*\}] \tag{106}$$

where

$$\eta_1(x) = \frac{i\underline{u}(r_1, x)}{(1-f) r_1}$$

[3]Other possible selection criteria for the c_k's are given in Reference 21. In most cases where the fit is good, the resulting computed side moment is essentially the same.

The pressure relation (28) assumes two forms, one for each side of the interface:

$$\begin{aligned}\frac{p-p_0}{\rho_L a^2\dot{\phi}^2} &= q_1\left[\frac{r^2-r_0^2}{2}-R\{\underline{p}K^*\}\right], \quad 0\,(or\ r_f\ or\ r_r)\le r\le r_i \\ &= q_1\left[\frac{r_i^2-r_0^2}{2}\right]+\frac{r^2-r_i^2}{2}-R\{\underline{p}K^*\}, \quad r_i\le r\le r_c \end{aligned} \tag{107}$$

where

$$q_1=\rho_2/\rho_1$$

Differential equations (52-57) become

$$Z'_{1k} = -Z_{2k}/r-\lambda_{k1}Z_{4k} \tag{108}$$

$$Z'_{2k} = -Z_{2k}/r-\lambda_{k1}Z_{4k}-iZ_{3k} \tag{109}$$

$$\begin{aligned}Z'_{3k} &= 2(q_{2r}Re+ir^{-2})Z_{1k}+i(B+r^{-2})(Z_{2k}-Z_{1k}) \\ &\quad -Z_{3k}/r-(iq_{2r}Re/r)Z_{6k}\end{aligned} \tag{110}$$

$$Z'_{4k} = Z_{5k} \tag{111}$$

$$Z'_{5k} = BZ_{4k}-Z_{5k}/r-\lambda_{k2}q_{2r}ReZ_{6k} \tag{112}$$

$$\begin{aligned}Z'_{6k} &= (q_{2r}Re)^{-1}[-BZ_{1k}+(2iq_{2r}Re-r^{-2})(Z_{2k}-Z_{1k}) \\ &\quad +iZ_{3k}/r-\lambda_{k1}Z_{5k}]\end{aligned} \tag{113}$$

where

$$\begin{aligned}B &= r^{-2}+\lambda_k^2-i(1-f)q_{2r}Re \\ q_{2r} &= q_2\equiv\nu_1/\nu_2 \quad r_0\le r\le r_1 \\ &= 1, \quad r_1<r\end{aligned}$$

At the interface, the velocities and stresses are continuous; therefore,

$$\underline{w}(r_1^-,x) = \underline{w}(r_1^+,x) \tag{114}$$

$$\underline{u}(r_1^-,x) = \underline{u}(r_1^+,x) \tag{115}$$

$$\underline{v}(r_1^-,x) = \underline{v}(r_1^+,x) \tag{116}$$

$$q_3(Re)^{-1}\left[\frac{\partial\underline{v}(r_1^-,x)}{\partial r}-\frac{i[\underline{u}(r_1^-,x)-i\underline{v}(r_1^-,x)]}{r_1}\right]=(Re)^{-1}\left[\frac{\partial\underline{v}(r_1^+,x)}{\partial r}-\frac{i[\underline{u}(r_1^+,x)-i\underline{v}(r_1^+,x)]}{r_1}\right] \tag{117}$$

$$q_3(Re)^{-1}\left[\frac{\partial\underline{w}(r_1^-,x)}{\partial r}+\frac{\partial\underline{u}(r_1^-,x)}{\partial x}\right]=(Re)^{-1}\left[\frac{\partial\underline{w}(r_1^+,x)}{\partial r}+\frac{\partial\underline{u}(r_1^+,x)}{\partial x}\right] \tag{118}$$

$$q_1\left[\underline{p}(r_1^-,x)+\frac{ir_1\underline{u}(r_1^-,x)}{1-f}-2(q_2Re)^{-1}\frac{\partial\underline{u}(r_1^-,x)}{\partial r}\right]=\underline{p}(r_1^+,x)+\frac{ir_1\underline{u}(r_1^+,x)}{1-f}-2(Re)^{-1}\frac{\partial\underline{u}(r_1^+,x)}{\partial r} \tag{119}$$

where

$$q_3=\frac{q_1}{q_2}=\frac{\mu_2}{\mu_1},$$

the ratio of the inner and outer dynamic viscosities. Thus the pressure perturbation $\underline{p}$ and the radial derivatives of $\underline{v}$ and $\underline{w}$ have jump discontinuities at the interface.

VII. Binary Solutions

1. Stewartson Inviscid Binary (SB) Solution

Eqs.(71-83) still apply, with the additional complication of a jump in the pressure term at the interface $r = r_1$. If we denote the binary perturbation functions for the pressure and velocity by Z_{1kB} and Z_{6kB}, Eqs.(115,119) reduce to

$$\Delta Z_{1kB} = 0 \tag{120}$$

$$\Delta Z_{6kB} = (q_1 - 1)\left[Z_{6kB}(r_1^-) + \frac{ir_1 Z_{1kB}(r_1^-)}{1-f} + \frac{ir_1 f}{2}\right] \tag{121}$$

where

$$\Delta(\ ) = (\ )_{r=r_1^+} - (\ )_{r=r_1^-}$$

These binary perturbation functions can be constructed from the single-liquid functions by the following device:

$$\begin{aligned} Z_{1kB}(r) &= Z_{1k}(r) + \hat{a}_k Z_{7k}(r), \quad r \le r_1 \\ &= Z_{1k}(r) + \hat{b}_k Z_{7k}(r), \quad r > r_1 \end{aligned} \tag{122}$$

$$\begin{aligned} Z_{6kB}(r) &= Z_{6k}(r) + \hat{a}_k Z_{12k}(r), \quad r \le r_1 \\ &= Z_{6k}(r) + \hat{b}_k Z_{12k}(r), \quad r > r_1 \end{aligned} \tag{123}$$

where the Z_{7k}'s and Z_{12k}'s are solutions of Eqs.(71-74) when each subscript 'nk' has been replaced by '(n+6)k' and the boundary conditions are

(a) in general:

$$\begin{aligned} Z_{7k}(r_1) &= 1 \\ Z_{7k}(1) &= 0 \end{aligned}$$

(b) for a fully-filled cylinder:

$$Z_{12k}(0) = 0$$

(c) for a partially-filled cylinder:

$$Z_{12k}(r_0) + \frac{ir_0 Z_{7k}(r_0)}{1-f} = 0$$

(d) for a cylinder with a central rod:

$$Z_{7k}(r_0) = 0$$

Note that Z_{12k} has a jump discontinuity at r_1. The Z_{7k} and Z_{12k} functions can be computed by two calls to the SUPORT code: for $0 < r \le r_1$ (or $r_0 \le r \le r_1$) and for $r_1 \le r \le 1$. The $\hat{a}_k$'s and $\hat{b}_k$'s are determined by Eqs.(120-121):

$$\hat{a}_k = \hat{b}_k \tag{124}$$

$$\hat{b}_k \left[Z_{12k}(r_1^+) - q_1 Z_{12k}(r_1^-) + \frac{i(1-q_1)r_1}{1-f} \right] = (q_1 - 1) \left[Z_{6k}(r_1) + \frac{ir_1 Z_{1k}(r_1)}{1-f} + \frac{ir_1 f}{2} \right] \quad (125)$$

Equations similar to (124-125) were used by Scott[28] to obtain eigenfrequencies τ_k for which the inviscid liquid moment was infinite.

2. Stewartson-Wedemeyer Binary (SWB) Solution

If $\nu_2 \neq \nu_1$, the SWB method must use an average kinematic viscosity; this average was chosen to be

$$\nu_a = \frac{\nu_2(r_1^2 - r_0^2) + \nu_1(1 - r_1^2)}{1 - r_0^2} \quad (126)$$

From this, an average Reynolds number, Re_a, and an average value, δ_{ca}, of δ_c can be determined; the eigenvalues can then be computed from Eq.(87) for this average value. An approximation for these eigenvalues is

$$\lambda_k \approx \frac{k\pi}{2(A - \delta_{ca})} \quad (127)$$

Next, two additional boundary layers are inserted at the interface to satisfy the continuity of the tangential stress, Eqs.(65-66). This, however, requires a discontinuity in the inviscid radial velocity, since the outflow in the two boundary layers are not equal. Eqs.(120-121) have new jump values in terms of the Stewartson pressure jump $(\Delta Z_{6kB})_S$:

$$\Delta Z_{1kB} = (1 - q_1)\delta_a F \quad (128)$$

$$\Delta Z_{6kB} = (\Delta Z_{6kB})_S - \frac{ir_1 \Delta Z_{1kB}}{1 - f} \quad (129)$$

where

$$F = \left\{ (1 + e_3^2)\Delta Z'_{1k} - \frac{2e_3}{r_1} \left[\frac{\partial(rZ_{1k})}{\partial r} \right]_{r=1} - \frac{2ie_3}{r_1} \right\} e_4^{-1}$$

$$e_3 = exp[(r_1 - 1)/\delta_a]$$

$$e_4 = q_2^{1/2}[1 + q_5 + (1 - q_5)e_3^2] - (1 - q_1)(1 + e_3^2)\delta_a$$

$$q_5 = q_1/q_2^{1/2}$$

Note that Eqs.(128-129) reduce to Eqs.(120-121) for $\delta_a = 0$. The SWB equations in this report are based on the assumption that the radial thickness of the inner liquid is substantially greater than the boundary layer thickness; that is, $r_1 - r_0 >> |\delta_a|$. Reference 7 considers the case where this assumption is invalid.

Finally, the presence of boundary layers on the cylinder wall and on the rod requires new conditions on $Z_{1k}(1)$ and $Z_{7k}(1)$ for all cases:

$$Z_{1k}(1) - \left(\frac{\delta_a e_5}{1 - \delta_a e_5} \right) Z'_{1k}(1) = 1 - (2e_3 q_5 \delta_a / e_6)\Delta \frac{\partial(rZ_{1k})}{\partial r} \quad (130)$$

$$Z_{7k}(1) - \left(\frac{\delta_a e_5}{1 - \delta_a e_5} \right) Z'_{7k}(1) = -(2e_3 q_5 \delta_a / e_6)\Delta \frac{\partial(rZ_{7k})}{\partial r} \quad (131)$$

where

$$\begin{aligned} c_5 &= [1 + q_5 - (1 - q_5)c_3^2]/[1 + q_5 + (1 - q_5)c_3^2] \\ c_6 &= [1 + q_5 + (1 - q_5)c_3^2][1 - c_5\delta_a] \end{aligned}$$

and on $Z_{1k}(r_0)$ and $Z_{7k}(r_0)$ for the rod:

$$Z_{1k}(r_0) + \left(\frac{r_0\delta_b}{r_0 + \delta_b}\right) Z'_{1k}(r_0) = 1 \tag{132}$$

$$Z_{7k}(r_0) + \left(\frac{r_0\delta_b}{r_0 + \delta_b}\right) Z'_{7k}(r_0) = 0 \tag{133}$$

where $\delta_b = \delta_a q_2^{-1/2}$.

Murphy[7] used equations similar to (128) and (129) to compute liquid moments that showed excellent agreement with experiment.

3. KGS Binary (KGSB) Solution

The KGSB solution uses the simple eigenvalues of Eq.(127) but requires the use of jump conditions (117-118) in addition to the pressure jump conditions given by Eq.(119) or (121). The three jump conditions for k = 1,2,...,N are

$$Z_{3kB}(r_1^+) - Z_{3kB}(r_1^-) = \Delta Z_{3kB} \tag{134}$$

$$Z_{5kB}(r_1^+) - Z_{5kB}(r_1^-) = \Delta Z_{5kB} \tag{135}$$

$$Z_{6kB}(r_1^+) - Z_{6kB}(r_1^-) = \Delta Z_{6kB} \tag{136}$$

where

$$\begin{aligned} \Delta Z_{3kB} &= (q_3 - 1)[Z_{3kB}(r_1^-) - iZ_{2kB}(r_1)/r_1] \\ \Delta Z_{5kB} &= (q_3 - 1)[Z_{5kB}(r_1^-) - \lambda_k Z_{1kB}(r_1) + \lambda_k] \end{aligned}$$

and where ΔZ_{6kB} is defined in Eq.(121).

In order to satisfy conditions (134-136), we need to introduce three sets of six auxiliary functions, defined in Table 3. These functions are continuous in the velocity components. Substitution in Eqs.(134-136) yields the values of d_k, e_k, and f_k. The resulting values of $(Z_{ikB})_{i=1...6}$ can then be used to compute the liquid moment exerted by a binary liquid payload.

4. HSG Binary (HSGB) Solution

In the KGSB solution, $\hat{w}_0, \hat{u}_0, \hat{v}_0$, and $\hat{p}_0$ were zero and the auxiliary functions of Table 3 were used for positive k. For HSGB, the binary λ_0 eigenfunctions must also be computed by use of the auxiliary functions given in Table 3. The jump conditions for the λ_0 eigenfunctions are

$$\Delta Z_{30B} = (q_3 - 1)[Z_{30B}(r_1^-) - iZ_{20B}(r_1)/r_1] \tag{137}$$

$$\Delta Z_{50B} = (q_3 - 1)[Z_{50B}(r_1^-) - Z_{10B}(r_1) + 1] \quad (138)$$

$$\Delta Z_{60B} = (q_1 - 1)\left[Z_{60B}(r_1^-) + \frac{ir_1 Z_{10B}(r_1)}{1-f} + \frac{ir_1 f}{2}\right] - \frac{2(q_3-1)Z'_{10B}(r_1)}{Re} \quad (139)$$

The jump conditions for the other eigenfunctions (k = 1,2,..., N) are

$$\Delta Z_{3kB} = (q_3 - 1)[Z_{3kB}(r_1^-) - iZ_{2kB}(r_1)/r_1] \quad (140)$$

$$\Delta Z_{5kB} = (q_3 - 1)[Z_{5kB}(r_1^-) - \lambda_k Z_{1kB}(r_1)] \quad (141)$$

$$\Delta Z_{6kB} = (q_1 - 1)\left[Z_{6kB}(r_1^-) + \frac{ir_1 Z_{1kB}(r_1)}{1-f}\right] - \frac{2(q_3-1)Z'_{1kB}(r_1)}{Re} \quad (142)$$

These jump conditions are used to determine the necessary d_k's, e_k's and f_k's. The resulting binary eigenfunctions are then used to satisfy the end-wall boundary conditions of Eqs.(101-103); that is,

$$\sum_{k=1}^{N} c_k Z_{1kB}(r) g_k = R_1 \equiv A\hat{f}[1 - Z_{10B}(r)] \quad (143)$$

$$\sum_{k=1}^{N} c_k Z_{2kB}(r) g_k = R_2 \equiv -A\hat{f} Z_{20B}(r) \quad (144)$$

$$\sum_{k=1}^{N} c_k Z_{4kB}(r) h_k = R_3 \equiv -\hat{f} Z_{40B}(r) \quad (145)$$

The c_k's are then selected to fit Eqs.(143-145) so that R is minimized, where

$$R = \int_{r_0}^{1} q_{1r}\{|\sum c_k Z_{1kB} - R_1|^2 + |\sum c_k Z_{2kB} - R_2|^2 + |\sum c_k Z_{4kB} h_k - R_3|^2\} r\, dr \quad (146)$$

and where

$$q_{1r} = q_1 \quad (r \le r_1)$$
$$= 1 \quad (r > r_1)$$

The error of the fit is computed by Eq.(105) with

$$R_0 = \int_{r_0}^{1} q_{1r}\{|R_1|^2 + |R_2|^2 + |R_3|^2\} r\, dr$$

VIII. Liquid Moment

If a projectile is performing simple coning motion, the moment exerted on it by a fully spun-up liquid payload can be defined in terms of three dimensionless moment coefficients. These coefficients are related to the liquid moment (M_{xc}, M_{yc}, M_{zc}) in the coning coordinate system as follows:

$$M_{xc} = m_L a^2 \dot{\phi}^2 \tau C_{LRM} K^2 \quad (147)$$

$$M_{yc} + iM_{zc} = m_L a^2 \dot{\phi}^2 \tau [C_{LSM} + iC_{LIM}] K \quad (148)$$

where

$$m_L = 2\pi a^2 c \rho_L$$

These three coefficients - the liquid roll moment coefficient C_{LRM}, the liquid side moment coefficient C_{LSM}, and the liquid in-plane moment coefficient C_{LIM} - are all functions of A, τ, ϵ, Re and K^2. The liquid side moment affects the damping of the coning motion while the liquid in-plane moment can cause a frequency shift. Thus our primary interest is in the liquid side moment coefficient C_{LSM} since it determines any instabilities that could occur.

The linear pressure at any point of the cylinder can be expressed in the coning coordinates by combining Eqs.(10,11,107):

$$\begin{aligned} \frac{p - p_0}{\rho_L a^2 \dot{\phi}^2} &= q_1 \left[\frac{\tilde{r}^2 - r_0^2}{2} - R\{(\underline{p} + \tilde{x}\tilde{r})K^*\} \right], \quad 0\ (or\ \tilde{r}_f\ or\ \tilde{r}_r) \le \tilde{r} \le \tilde{r}_i \\ &= q_1 \left[\frac{r_1^2 - r_0^2}{2} \right] + \frac{\tilde{r}^2 - r_1^2}{2} - R\{(\underline{p} + \tilde{x}\tilde{r})K^*\}, \quad \tilde{r}_i \le \tilde{r} \le 1 \end{aligned} \tag{149}$$

The linear coefficient of K^* is defined as the pressure coefficient C_p and can be expressed in terms of $Z_{6k}(r)$ by use of Eqs.(36,51):

$$C_p = q_{1r} f[(2 - f)xr + \sum_{k=0}^{N} c_k Z_{6k}(r) G_k(x)] \tag{150}$$

Note that the distinction between x, r and $\tilde{x}, \tilde{r}$ vanishes in the linear terms.

The linear coefficients can be computed from the fluid mechanics theory of this report by integrating the pressures and viscous stresses over the lateral cylindrical wall and the two flat end-walls. If a central rod is present, its pressure and viscous contributions must also be included. Using subscripts p for pressure, v for viscous, ℓ for lateral wall, e for end wall and r for rod, we have[4,12]

$$C_{LSM} + iC_{LIM} = C_{mp\ell} + C_{mpe} + C_{mpr} + C_{mv\ell} + C_{mve} + C_{mvr} \tag{151}$$

Expressions for the components in Eq.(151) are given in Table 4 for HSG and HSGB. The table also applies to the S and SB theories when the Reynolds number is infinite, but additional terms must be introduced for the boundary layer theories (SW, SWB, KGS, KGSB), as indicated in Table 5.

The linear fluid moments can also be computed directly by differentiating the volume integral of the angular momentum of all the liquid in the cylinder. To do this, we first express the position and velocity vectors in earth-fixed cylindrical coordinates ($\hat{e}_x, \hat{e}_r, \hat{e}_\theta$):

$$\vec{R} = (x\hat{e}_x + r\hat{e}_r)a \tag{152}$$

$$\vec{V} = V_x\hat{e}_x + V_r\hat{e}_r + V_\theta\hat{e}_\theta \tag{153}$$

$$\begin{aligned} \hat{e}_r &= \hat{e}_y \cos\theta + \hat{e}_z \sin\theta \\ &= (-K\hat{e}_{xc} + \gamma\hat{e}_{yc})\cos\psi + \hat{e}_{zc}\sin\psi \end{aligned} \tag{154}$$

$$\begin{aligned} \hat{e}_\theta &= \hat{e}_x \times \hat{e}_y \\ &= (K\hat{e}_{xc} - \gamma\hat{e}_{yc})\sin\psi + \hat{e}_{zc}\cos\psi \end{aligned} \tag{155}$$

Then

$$\vec{R} \times \vec{V} = [rV_\theta \hat{e}_x - xV_\theta \hat{e}_r + (xV_r - rV_x)\hat{e}_\theta]a \tag{156}$$

The angular momentum is

$$\begin{aligned} \vec{L} &= a^3 \int_0^1 \int_{-A}^{A} \int_0^{2\pi} \rho \vec{R} \times \vec{V} \tilde{r}\, d\tilde{r}\, d\tilde{x}\, d\tilde{\psi} \\ &= L_1 \hat{e}_{xc} + L_2 \hat{e}_{yc} + L_3 \hat{e}_{xc} \end{aligned} \tag{157}$$

where expressions for the L_j are given in Table 6.

The moment exerted by the liquid on the projectile is the negative of the derivative of the liquid's angular momentum:

$$\begin{aligned} \vec{M} &= -\dot{\vec{L}} \\ &= -(\dot{L}_1 \hat{e}_{xc} + \dot{L}_2 \hat{e}_{yc} + \dot{L}_3 \hat{e}_{xc} + \vec{\Omega} \times \vec{L}) \end{aligned} \tag{158}$$

For steady-state constant-amplitude liquid motion,

$$\dot{L}_j = \epsilon = 0 \tag{159}$$

$$\begin{aligned} \vec{M} &= -\tau \dot{\phi} \hat{e}_x \times \vec{L} \\ &= \tau \dot{\phi}[-KL_3 \hat{e}_{xc} + \gamma L_3 \hat{e}_{yc} + (KL_1 - \gamma L_2)\hat{e}_{xc}] \end{aligned} \tag{160}$$

Eq.(160) - applied to definitions (147-148) - yields the very important result that

$$\gamma C_{LRM} = -C_{LSM} \tag{161}$$

This result has been obtained elsewhere[9,18], but the above is the simplest, most direct derivation and is based solely on the assumption of steady-state, constant-amplitude motion given by Eq.(159).

The first terms in an expansion in K of the L_j's, obtained by use of Eqs.(16-18), are given in Table 6. Substituting these small-K expressions for the L_j's in Eq.(158), we obtain

$$C_{LRM} \approx -R\{\hat{S}\} \tag{162}$$

$$C_{LSM} + iC_{LIM} = (1 - i\epsilon)(\hat{S} + 2iB_1) \tag{163}$$

Since C_{LRM} is a quadratic coefficient, it can't generally be computed from a linear theory. Eq.(162) neglects the nonlinear part of $\dot{L}_1$. For $\dot{L}_1 = 0$, Eq.(162) gives the correct quadratic coefficient.

It is easy to show that $\hat{S}$ vanishes for $f = 0$. Therefore, for $\tau = \epsilon = 0$,

$$C_{LSM} = C_{LRM} = 0 \tag{164}$$

$$C_{LIM} = 2B_1 \tag{165}$$

Values of $C_{LSM} + iC_{LIM}$ obtained by this angular momentum approach will be denoted as C_{mm}. The appropriate formulas are given in Table 7; the derivation of these formulas is given in Appendix B.

IX. Numerical Results

1. Surface Integral versus Volume Integral

In the HSG, KGS and SW theories, the liquid moments were originally computed by integrating the pressure and wall shears over the walls of the container (see Tables 4 and 5). The volume integral method (Table 7) should give the same results if the velocity perturbation functions satisfy the linearized Navier-Stokes equations and the boundary conditions. For a sufficient number of eigenfunctions, this is the case for the HSG theory: the two values of C_{LSM} are equal. In Figure 2, C_{LSM} values obtained from HSG by both the surface and volume integral methods are plotted versus the number of eigenvalues used, for Re = 500, A = 3.1 and $\tau = 0.1$. For 28 eigenvalues or more, the values from the two methods are essentially equal. For a smaller number of eigenvalues, the two values differ, but the volume integral result is always closer to their common value for more than 28 eigenvalues. This figure also shows the error of the fit to the end-wall boundary condition; we see that the C_{LSM} are the same when the error is less than 0.10.

Gans[29] uses the volume integral method in his version of SW and he notes that this method correctly predicts that the side moment coefficient goes to zero as τ goes to zero, whereas SW results based on the surface integral method do not have this property. Both Rosenblat[12] in his finite element calculations and Herbert[13] in his spectral method use the volume integral approach. Herbert emphasizes the value of the volume integral in giving better results for the approximate theories. Indeed, for the approximate boundary layer theories at low Reynolds numbers, the average error in velocity predictions should be much less than the error in the velocity gradients at the boundary.

In Figure 3, the volume and surface integral results for KGS and SW are compared at Re = 500, A = 3 and τ ranging from 0 to 0.20. The exact HSG values are also given in the figure. The surface integral results are essentially worthless, but the volume integral results are quite good, with KGS somewhat better than SW. For this reason, we will routinely use the volume integral to compute the liquid moments for all theories.

2. Fully Filled Cylinders

Historically, our interest in the moment produced by highly viscous liquids is based on experiments by Miles Miller[31]. He measured the liquid roll moment in a coning, spinning, liquid-filled cylinder and showed that at a Reynolds number of about 150, the liquid roll moment was large enough to cause flight instabilities[31]. The theoretical basis for this very important result is Eq.(161), which directly relates the liquid roll moment of Miller's experiments to the liquid side moment that controls flight instabilities.

In Figure 4, we plot the negative of Miller's[32-33] C_{LRM} versus $log_{10}Re$ for a fully filled cylinder of fineness ratio 4.5 and $\tau = 0.1$. This figure also gives the HSG, KGS and SW curves for C_{LSM}. For HSG and KGS, we see good qualitative agreement but poor quantitative agreement with the Miller data for Re less than about 20.

The most striking feature revealed by Figure 4 is the exceptional ability of the KGS

theory to predict the much more soundly based HSG curve. The three theories are compared for two other fineness ratios, 3 and 1.5, in Figures 5 and 6, respectively, and we see that the excellent agreement for the KGS theory persists for all Reynolds numbers greater than unity. The SW theory, however, does surprisingly well down to an Re of 100. Previous comparisons showed poor agreement for Re less than 1000. The primary difference between the earlier computations and those of Figures 4-6 is that Figures 4-6 were obtained by (a) using the volume integral method, (b) adding the special eigenvalue (see page 10), and (c) imposing a more exact boundary condition, Eq.(C19).

The SW method results in a very fast computer code since it is based on linear combinations of easily generated Bessel functions. Indeed, three-dimensional surfaces of C_{LSM} as functions of any *two* of the parameters $(\tau, \epsilon, Re, A, r_0)$ can be obtained quickly in the interactive mode on our VAX 8600.

The KGS method solves a sixth-order complex differential equation numerically for a set of eigenvalues. These eigenvalues are quite easy to compute; usually, less than twelve are required to satisfy the boundary conditions adequately. For Re less than 1000, a single calculation of C_{LSM} takes less than 15 seconds on our VAX, but the run time increases with Reynolds number. The very exact HSG method unfortunately requires many more eigenvalues (our code has an arbitrary, but easily extendable, limit of 72). These eigenvalues are computed from tables of starting estimates and an iterative Newton scheme.

The agreement between the theories as demonstrated by Figures 4-6 has a very important pay-off. For Reynolds numbers greater than 300, the improved SW method of this report can be used to compute C_{LSM} in a very fast interactive code. For Re between 0 and 300, HSG results can be reasonably well approximated by the KGS code, a process somewhat slower than the SW program but still fully interactive.

This ability to obtain C_{LSM} rapidly over a wide spectrum of Re values is demonstrated by Figure 7, a three-dimensional plot of C_{LSM}. versus Re and τ, for a fully filled cylinder of fineness ratio 4.5. The plot was obtained from the KGS and SW codes. For the higher Reynolds numbers, we see the characteristic resonance peak at about $\tau = 0.20$. For a fixed τ, a mild peak appears near Re = 50. Similar 3D figures were first made by Miller[32].

An important feature of Figure 3 that has not yet been addressed is the linearity of C_{LSM} with τ for τ less than 0.2. According to Eq.(148), a linear C_{LSM} implies a side moment that varies as the square of the coning frequency and is *independent* of the spin rate.

The region of linearity in τ can be characterized by the slopes k_S and k_R, where

$$C_{LSM} = k_S \tau, \quad C_{LRM} = k_R \tau$$

and by τ_m, the maximum value of τ for which linearity is valid. We will define τ_m to be the lowest positive τ value for which C_{LSM}/τ falls outside the interval $0.9k_S$ to $1.1k_S$. In Figures 8 and 9, we plot k_S and τ_m, respectively, versus Re for Re between 0 and 1000. As can be seen from Figure 9, for $Re < 250$ the side moment coefficient is linear with τ for a substantial τ range (viz., $\tau < 0.2$). This is precisely the experimental observation by Miller[31] for the liquid roll moment.

3. Partially Filled Cylinders and Central Rods

Stewartson's original inviscid work[1] and Wedemeyer's viscous extension[2] covered both fully and partially filled cylinders. Frasier[3] extended the SW theory to a cylindrical cavity with a central rod. Both the KGS and HSG theories[10-13,21] were originally restricted to fully filled cylindrical cavities. With the help of the very general SUPORT subroutine[26], it is quite easy to extend the KGS theory to partially filled cavities and central rods; this has been done for this report. As mentioned earlier, the extension of the HSG theory to these cases requires the forming of additional files of eigenvalues. These eigenvalues have been obtained, using BRL's CRAY supercomputers.

For Figure 10, the side moment coefficient has been computed by all three theories for a partially filled cylinder of fineness ratio 3, with a Reynolds number of 500 and $\tau = 0.10$, and plotted against the inner cylindrical free surface ratio b/a. As we would expect, the side moment vanishes when this ratio is 1.0 and the cavity is empty. The generation of HSG eigenfunctions gets to be too tedious for $b/a > 0.9$, but we see that the KGS theory is a good approximation to the more exact HSG theory in the range $0 < b/a < 0.9$.

Figure 11 is a similar plot for the central rod ratio d/a varying from 0 to 1. The HSG eigenfunctions were only calculated for d/a up to 0.5. Once again, the computationally simpler KGS theory is a good approximation to the HSG theory. Thus for most engineering calculations, the KGS theory would be the one to use.

4. Binary Liquids

The SW theory was extended to binary liquids (SWB) in Reference 7. The extension of the KGS and HSG theories to their binary versions, KGSB and HSGB, has been done as part of this report. The eigenfunctions and boundary conditions for the KGSB theory are essentially the same as those for the KGS theory; hence the eigenfunctions have no difficulty fitting the lateral wall condition, Eq.(59). The HSG end-wall boundary condition, Eq.(104), can be reasonably well satisfied by ten HSG eigenfunctions at Re = 10 and by less than 72 HSG eigenfunctions for Re less than 2000. Unfortunately, this is not the case for the HSGB boundary condition of Eq.(146) and the HSGB eigenfunctions. Even for quite low Reynolds numbers, a large number of eigenfunctions is required. For this reason, we have stopped (at least temporarily) running our HSGB program.

The great success of the KGS theory, however, allows us to place primary reliance on the KGSB theory to calculate the effect of binary liquids of different densities and/or viscosities on the liquid side moment. For high Reynolds number, good experimental agreement has been obtained[34]; the validity of the KGSB theory at lower Reynolds numbers will depend on future experiments.

In Figure 12, C_{LSM} is plotted against τ for a cylindrical cavity containing approximately equal amounts of liquid ($r_1^2 = 0.49$), the densities of the two liquids differing by 60% ($\rho_2 = 0.4\rho_1$) while the kinematic viscosities are equal. The two curves are for two kinematic viscosity values, corresponding to Reynolds numbers of 300 and 500. The interface is at $r_1 = 0.7$, the fineness ratio is 3.

In Figure 13, we restrict ourselves to Re = 500, A = 3, and $\tau = 0.15$, but vary the density ratio q_1 from 0 to 1. The two curves are for $r_1 = 0.5$ and $r_1 = 0.7$. The HSG value for one liquid ($q_1 = 1$) is plotted and we see that the agreement is quite good. (It is a wise practice to confirm KGSB calculations, where possible, with an HSG check point.)

Finally, in Figure 14 we consider a case where the inner liquid is very viscous and comprises 98% of the cylinder volume ($r_1 = 0.99$). The small amount of outer liquid has the same density but quite different viscosity. (In any experiment, the density of the outer liquid would have to be slightly greater than that of the principal liquid so that the outer liquid would be located near the cylindrical wall.) According to Figure 4, for A = 4.5 and $\tau = 0.1$, the maximum side moment coefficient occurs at an Re of approximately 50. Hence in Figure 14, we set A = 4.5, $\tau = 0.1$ and Re(inner liquid) = 50 and we vary q_2 from 0.1 to 100. Note that the side moment coefficient essentially vanishes when the Reynolds number of the outer liquid is 5000. This qualitative behavior has been observed by Miller. It is interesting to note that for the second curve (A = 3), the side moment is relatively insensitive to q_2.

X. Summary

1. The four liquid payload theories - S, SW, KGS and HSG - have been developed here in a single theoretical framework.

2. A very simple and elegant derivation of the relation between liquid side moment and liquid roll moment is given.

3. Moment coefficients have been computed by both surface integral and volume integral and the clear superiority of the volume integral is demonstrated.

4. Eigenvalue tables for a wide range of τ's and Reynolds numbers have been generated to allow quicker HSG calculation of the side moment coefficient. These tables originally applied only to a fully filled cylindrical cavity but they have been expanded to include partially filled cylinders and cylinders with a central rod.

5. Side moment coefficients computed from the more convenient KGS theory are shown to be good approximations to those obtained by the more exact HSG theory. This agreement is shown to exist not only for fully filled cylinders but for partially filled cylinders and cylinders with a central rod as well.

6. Although the binary version of HSG often fails to satisfy the end-wall boundary condition, the binary version of KGS does not have this difficulty and gives good agreement with experiments at high Reynolds numbers.

7. KGSB, the binary version of KGS, was used to determine the effect of a small amount of lower viscosity liquid on the side moment. The theory predicts the large decrease in side moment that has been observed experimentally.

Table 1. The Stewartson Z_{jk}'s as Bessel Functions

$$Z_{1k} = \frac{i\lambda_k}{(1-f)f_b}[E_k J_0 + F_k Y_0] + \frac{i}{(3-f)r}[E_k J_1 + F_k Y_1]$$

$$Z_{2k} = -\frac{if_b\lambda_k}{3-f}[E_k J_0 + F_k Y_0] + \frac{2i}{(3-f)r}[E_k J_1 + F_k Y_1]$$

$$Z_{3k} = -\frac{f_b\lambda_k}{(3-f)r}[E_k J_0 + F_k Y_0] + \left[\frac{2}{(3-f)r^2} - \frac{2\lambda_k^2}{(1-f)^2}\right][E_k J_1 + F_k Y_1]$$

$$Z_{4k} = \frac{i\lambda_k}{1-f}[E_k J_1 + F_k Y_1]$$

$$Z_{5k} = \frac{if_b\lambda_k^2}{1-f}[E_k J_0 + F_k Y_0] - \frac{i\lambda_k}{(1-f)r}[E_k J_1 + F_k Y_1]$$

$$Z_{6k} = E_k J_1 + F_k Y_1$$

where
$f_b = \sqrt{(3-f)(1+f)}/(1-f)$

$J_n = J_n(f_b\lambda_k r)$

= Bessel function of the first kind of order n

$Y_n = Y_n(f_b\lambda_k r)$

= Bessel function of the second kind of order n

and where the E_k's and F_k's are determined by the boundary conditions.
The condition $Z_{1k}(1) = 1$, for example, requires that

$$[(1-f)f_b\lambda_k J_{0a} + (1+f)J_{1a}]E_k + [(1-f)f_b\lambda_k Y_{0a} + (1+f)Y_{1a}]F_k = -i(3-f)(1+f)$$

where the subscript 'a' on a Bessel function denotes the value at r = 1.
For the fully-filled case, the condition $Z_{6k}(0) = 0$ requires that $F_k = 0$.

Table 2. Eigenvalues for a fully-filled cylinder, Re = 10, $\tau = 0$.

j	– Family 1 –	– Family 2 –	– Family 3 –
1	.904, 4.290	1.962, -3.697	1.309, 1.518
2	.573, 7.528	1.925, -6.702	2.837, 6.690
3	.415, 10.796	1.983, -9.791	2.567, 9.787
4	.326, 14.052	2.054, -12.891	2.484, 12.895
5	.269, 17.289	2.124, -15.997	2.463, 16.005
6	.229, 20.510	2.188, -19.109	2.468, 19.117
7	.200, 23.718	2.247, -22.225	2.485, 22.233
8	.177, 26.915	2.301, -25.346	2.508, 25.353
9	.159, 30.103	2.349, -28.470	2.533, 28.477
10	.144, 33.283	2.393, -31.598	2.558, 31.603
11	.132, 36.458	2.433, -34.727	2.583, 34.732
12	.121, 39.628	2.469, -37.859	2.606, 37.863
13	.112, 42.793	2.501, -40.992	2.628, 40.996
14	.104, 45.955	2.529, -44.127	2.648, 44.130
15	.096, 49.114	2.554, -47.263	2.665, 47.266
16	.090, 52.270	2.575, -50.401	2.680, 50.403
17	.084, 55.424	2.593, -53.539	2.693, 53.541
18	.078, 58.576	2.608, -56.679	2.703, 56.680
19	.073, 61.725	2.619, -59.820	2.710, 59.821
20	.069, 64.872	2.627, -62.962	2.714, 62.962
21	.064, 68.017	2.631, -66.105	2.715, 66.105
22	.060, 71.160	2.630, -69.250	2.712, 69.249
23	.055, 74.300	2.626, -72.396	2.705, 72.394
24	.051, 77.437	2.616, -75.544	2.694, 75.542

Table 3. Auxiliary Functions for the KGSB and HSGB Solutions

$$
\begin{aligned}
Z_{1kB}(r) &= Z_{1k} + d_k Z_{7k} + e_k Z_{13k} + f_k Z_{19k} \\
Z_{2kB}(r) &= Z_{2k} + d_k Z_{8k} + e_k Z_{14k} + f_k Z_{20k} \\
Z_{3kB}(r) &= Z_{3k} + d_k Z_{9k} + e_k Z_{15k} + f_k Z_{21k} \\
Z_{4kB}(r) &= Z_{4k} + d_k Z_{10k} + e_k Z_{16k} + f_k Z_{22k} \\
Z_{5kB}(r) &= Z_{5k} + d_k Z_{11k} + e_k Z_{17k} + f_k Z_{23k} \\
Z_{6kB}(r) &= Z_{6k} + d_k Z_{12k} + e_k Z_{18k} + f_k Z_{24k}
\end{aligned}
$$

The three sets $(Z_{jk})_{j=7\ldots12}$, $(Z_{jk})_{j=13\ldots18}$, $(Z_{jk})_{j=19\ldots24}$ satisfy the homogeneous form of the boundary conditions satisfied by the set $(Z_{jk})_{j=1\ldots6}$. At the interface:

for j = 7	13	19
$Z_{jk}(r_1) = 1$	0	0
$Z_{(j+1)k}(r_1) = 0$	1	0
$Z_{(j+3)k}(r_1) = 0$	0	1

Table 4. Liquid Moment Coefficients

$$C_{mp\ell} = i(1-i\epsilon)\left\{[f-2-c_0 Z_{60}(1)]A^2/3 - (1/2A)\sum c_k D_k Z_{6k}(1)\right\}$$

$$C_{mpe} = i(1-i\epsilon)\left[(2-f)B_1 + c_0\int_{r_0}^1 q_{1r} Z_{60}(r) r^2 dr + (1/A)\sum c_k g_k \int_{r_0}^1 q_{1r} Z_{6k}(r) r^2 dr\right]$$

$$C_{mpr} = -iq_1 r_0(1-i\epsilon)\left\{[(f-2)r_0 - c_0 Z_{60}(r_0)]A^2/3 - (1/2A)\sum c_k D_k Z_{6k}(r_0)\right\}$$

$$C_{mvl} = \frac{1-i\epsilon}{Re}\left\{c_0[iZ_{50}(1) - (A^2/3)Z_{30}(1)] + \sum c_k\left[\frac{ig_k Z_{5k}(1)}{\lambda_k A} - \frac{D_k Z_{3k}(1)}{2A}\right]\right\}$$

$$C_{mve} = \frac{i(1-i\epsilon)}{Re}\left\{-2\hat{f}B_2 + c_0\int_{r_0}^1 q_{3r}[2Z_{10}(r) - Z_{20}(r)]r\,dr + \sum c_k\lambda_k h_k\int_{r_0}^1 q_{3r}[2Z_{1k}(r) - Z_{2k}(r)]r\,dr\right\}$$

$$C_{mvr} = -\frac{q_3 r_0(1-i\epsilon)}{Re}\left\{c_0[ir_0 Z_{50}(r_0) - (A^2/3)Z_{30}(r_0)] + \sum c_k\left[\frac{ir_0 g_k Z_{5k}(r_0)}{\lambda_k A} - \frac{D_k Z_{3k}(r_0)}{2A}\right]\right\}$$

where all summations are for k = 1 to N and where

$B_1 = [1-(1-q_1)r_1^4 - q_1 r_0^4]/4$

$B_2 = [1-(1-q_3)r_1^2 - q_3 r_0^2]/2$

$c_0 = \hat{f}$ for HSG or HSGB

$= 0$ otherwise

$D_k = \int_{-A}^{A} xG_k(x)dx$

$q_{1r} = q_1 \quad (r \le r_1)$

$= 1 \quad (r > r_1)$

$q_{3r} = q_3 \equiv \frac{\mu_2}{\mu_1} \quad (r \le r_1)$

$= 1 \quad (r > r_1)$

$q_1 = q_3 = 1$ for a single liquid

Table 5. Boundary Layer Modifications to the Liquid Moment Coefficients

For SW, SWB, KGS and KGSB:

$$C_{mve} = \frac{(1-i\epsilon)i}{Re}\left\{-(1-\beta A)2\hat{f}B_2 + \sum_{k=1}^{N} c_k(\lambda_k h_k - \beta g_k)\int_{r_c}^{1} q_{3r}[2Z_{1k}(r) - Z_{2k}(r)]r\,dr\right\}$$

For SW and SWB:

In C_{mpl}, replace $Z_{6k}(1)$ by $Z_{6k}(1) - 2i\delta_a e_2 F_1(1)$

In C_{mpr}, replace $Z_{6k}(r_0)$ by $Z_{6k}(r_0) + 2i\delta_b e_2 F_1(r_0)$

In C_{mvl}, replace $Z_{5k}(1)$ by $Z_{5k}(1) - \delta_a^{-1} e_2 Z_{4k}(1)$
and replace $Z_{3k}(1)$ by $Z_{3k}(1) - i\delta_a^{-1} e_2 F_1(1)$

In C_{mvr}, replace $Z_{5k}(r_0)$ by $Z_{5k}(r_0) + \delta_b^{-1} e_2 Z_{4k}(r_0)$
and replace $Z_{3k}(r_0)$ by $Z_{3k}(r_0) + i\delta_b^{-1} e_2 F_1(r_0)$

where $\beta = (1+i)\sqrt{(1+f)Re_a/2}$
$F_1(r) = Z_{2k}(r) - Z_{1k}(r) + r$
$\delta_b = \delta_a q_2^{-1/2}$

Table 6. Components of the Liquid Angular Momentum

$\vec{L} = L_1\hat{e}_{xc} + L_2\hat{e}_{yc} + L_3\hat{e}_{zc}$

where

$L_j = a^4 \int_0^1 \int_{-A}^{A} \int_0^{2\pi} \rho(\tilde{r}) N_j \tilde{r}\, d\tilde{\psi}\, d\tilde{x}\, d\tilde{r}$

and where

$\rho(\tilde{r}) = 0, \quad 0 < \tilde{r} < \tilde{r}_f(\tilde{x}, \tilde{\psi})$

$= \rho_2, \quad \tilde{r}_f(\tilde{x}, \tilde{\psi}) < \tilde{r} < \tilde{r}_i(\tilde{x}, \tilde{\psi})$

$= \rho_1, \quad \tilde{r}_i(\tilde{x}, \tilde{\psi}) < \tilde{r} \leq 1$

$N_1 = \gamma r V_\theta + K[(xV_r - rV_x)\sin\psi + xV_\theta \cos\psi]$

$N_2 = KrV_\theta - \gamma[(xV_r - rV_x)\sin\psi + xV_\theta \cos\psi]$

$N_3 = (xV_r - rV_x)\cos\psi - xV_\theta \sin\psi$

For small K,

$L_1 = 2m_L a^2 \dot{\phi} B_1$

$L_2 = m_L a^2 \dot{\phi} K R\{i\hat{S}\}$

$L_3 = m_L a^2 \dot{\phi} K R\{\hat{S}\}$

where

$\hat{S} = I + (1 - q_1) f F_2(r_1) + q_1 q_4 f F_2(r_0)$

$I = -(1/2A) \int_{-A}^{A} \int_{r_0}^{1} q_{1r}[\tilde{r}(i\tilde{r} - \underline{w}) + \tilde{x}(\underline{u} + i\underline{v} + 2i\tilde{x}]\tilde{r}\, d\tilde{r} d\tilde{x}$

$f F_2(r) = -\frac{r^2}{2(1-f)A} \int_{-A}^{A} [\underline{u}(r, \tilde{x}) + i(1 - f)\tilde{x}]\tilde{x}\, d\tilde{x}$

$q_4 = 1$ for partial fill; zero otherwise

Table 7. Liquid Moment Coefficients Computed from the Angular Momentum

For HSG, HSGB, S and SB:

$$C_{mm} = (1 - i\epsilon)\{2iB_1 + f[F_3 + (1 - q_1)fF_2(r_1) + q_1(f + q_4 - 1)F_2(r_0)]\}$$

For KGS and KGSB, add:

$$(\Delta C_{mm})_1 = -(1 - i\epsilon)f\left\{[(A\beta - 1)/\beta^2]F_4 - (1 - f)F_2(1) - (1 - q_1)\hat{F}_2(r_1) - q_1q_4\hat{F}_2(r_0)\right\}$$

For SW, add $(\Delta C_{mm})_1$ plus

$$(\Delta C_{mm})_2 = -(1 - i\epsilon)f\delta_a EF_5(1)e_2$$

For a central rod, using SW, add $(\Delta C_{mm})_1$, $(\Delta C_{mm})_2$ and

$$(\Delta C_{mm})_3 = -(1 - i\epsilon)f\delta_b EF_5(r_0)e_2$$

All summations are for k = 1 to N and

$$B_3 = [1 - (1 - q_1)r_1^2 - q_1r_0^2]/2$$

$$E = 1 - e^{(r_0-1)/\delta_a}$$

$$F_2(r) = \frac{r^2}{2(1-f)}\left\{(2A^2/3)\left[\hat{f} - c_0Z_{10}(r)\right] - (1/A)\sum c_kD_kZ_{1k}(r)\right\}$$

$$\hat{F}_2(r) = -\frac{r^2}{2(1-f)}\left\{\frac{A\beta-1}{\beta^2}\left[2\hat{f} - (1/A)\sum c_kg_k[2Z_{1k}(r) - Z_{2k}(r)]\right] - \frac{A\alpha-1}{\alpha^2A}\sum c_kg_kZ_{2k}(r)\right\}$$

$$F_3 = -i(B_1 + 2B_3A^2/3) - c_0I_0 + \sum c_kI_k(h_k - 2g_k/A\lambda_k)$$

$$F_4 = 2\hat{f}B_3 - (1/A)\sum c_gg_k\hat{I}_k$$

$$F_5(r) = r\left\{\hat{f}A^2/3 + (1/2A)\sum c_k\{D_k[Z_{2k}(r) - Z_{1k}(r)] - 2rg_kZ_{4k}(r)/\lambda_k\}\right\}$$

$$I_k = \int_{r_0}^1 q_{1r}Z_{4k}(r)r^2\,dr$$

$$\hat{I}_k = \int_{r_0}^1 q_{1r}[2Z_{1k}(r) - Z_{2k}(r)]r\,dr$$

$$\alpha = -i\beta\sqrt{(3 - f)/(1 + f)}$$

$$\delta_b = \delta_a q_2^{-1/2}$$

Table 8. Liquid Moment Coefficient Differences for Partial Fill and $L \neq 0$

$$\Delta C_{mpl}/L^2 = -i(1-ie)[f - Z_{6L}(1) + (1/A)\sum \lambda_k^{-1} c_{Lk} Z_{6k}(1)$$

$$\Delta C_{mwl}/L^2 = (1-ie)(Re)^{-1}[Z_{3L}(1) - (1/A)\sum \lambda_k^{-1} c_{Lk} Z_{3k}(1)$$

$$\Delta C_{mpr}/L^2 = ir_0(1-ie)[fr_0 - Z_{6L}(r_0) + (1/A)\sum \lambda_k^{-1} c_{Lk} Z_{6k}(r_0)$$

$$\Delta C_{mwr}/L^2 = -r_0(1-ie)(Re)^{-1}[Z_{3L}(r_0) - (1/A)\sum \lambda_k^{-1} c_{Lk} Z_{3k}(r_0)$$

where all summations are for k = 1 to N

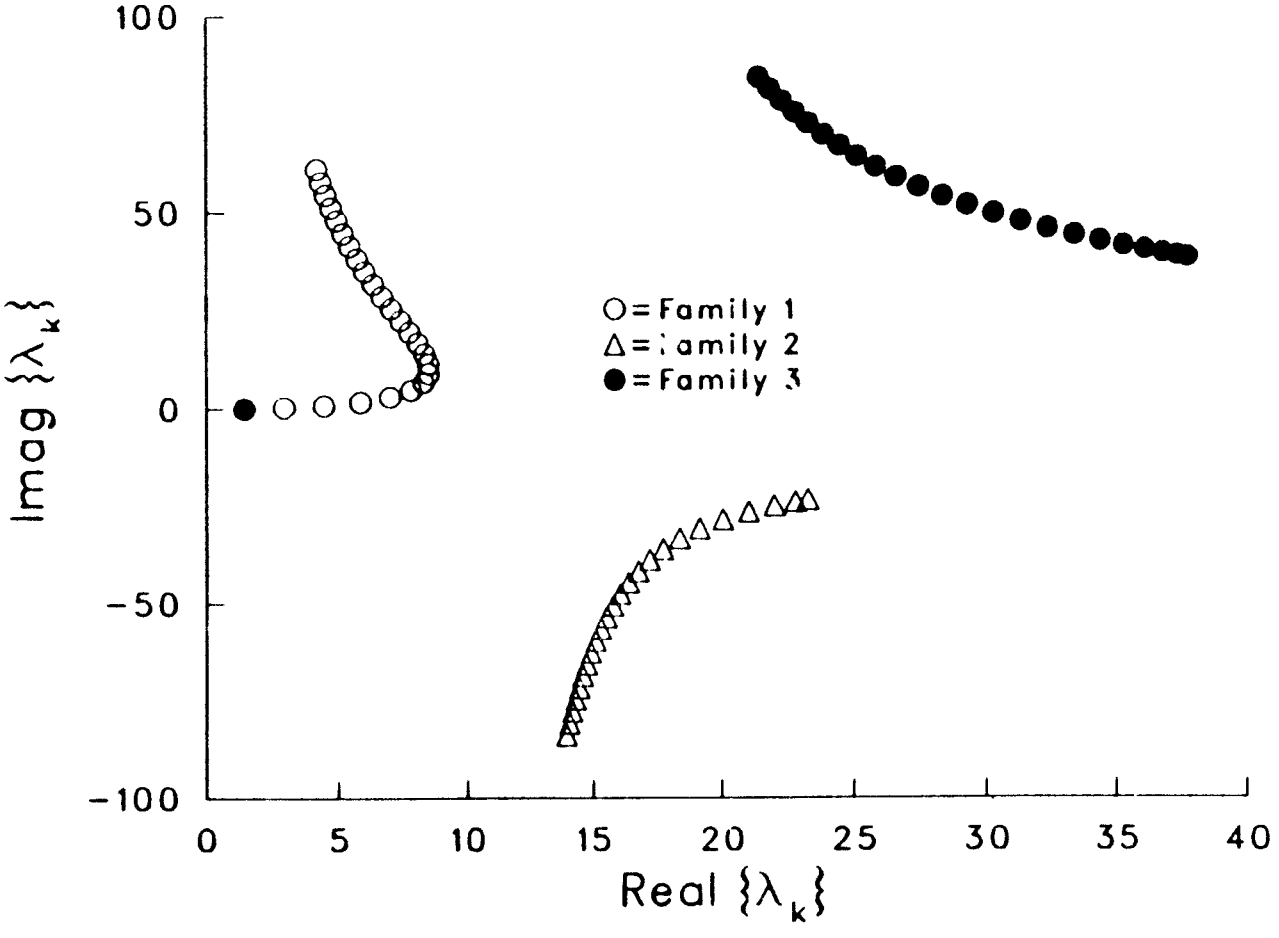

Fig. 1. Eigenvalues for a fully filled cylinder, Re = 1000, τ = 0.1

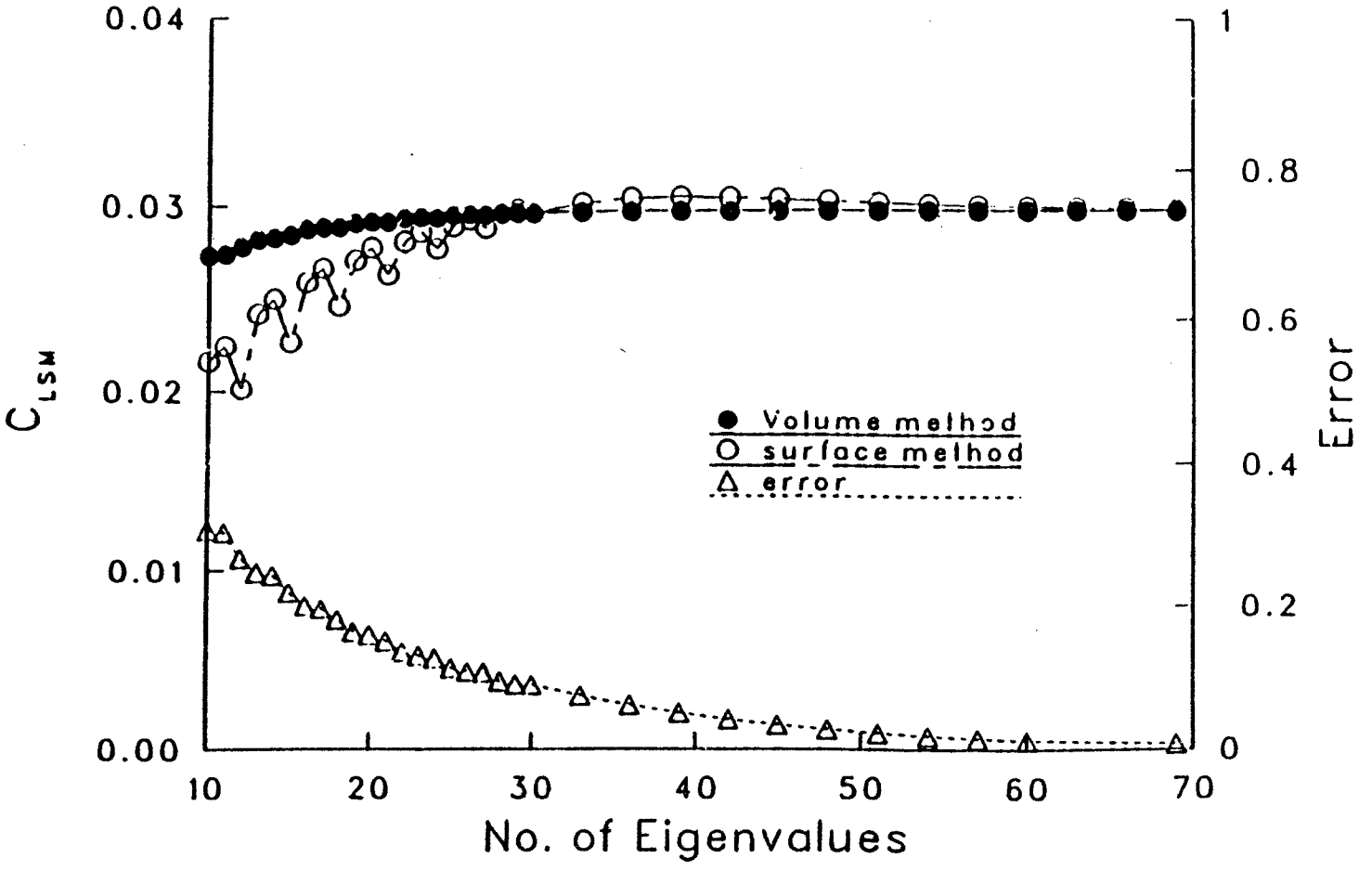

Figure 2. C_{LSM} (by HSG, volume and surface methods) vs. no. of e.v.'s (Re = 500, A = 3, τ = 0.1).

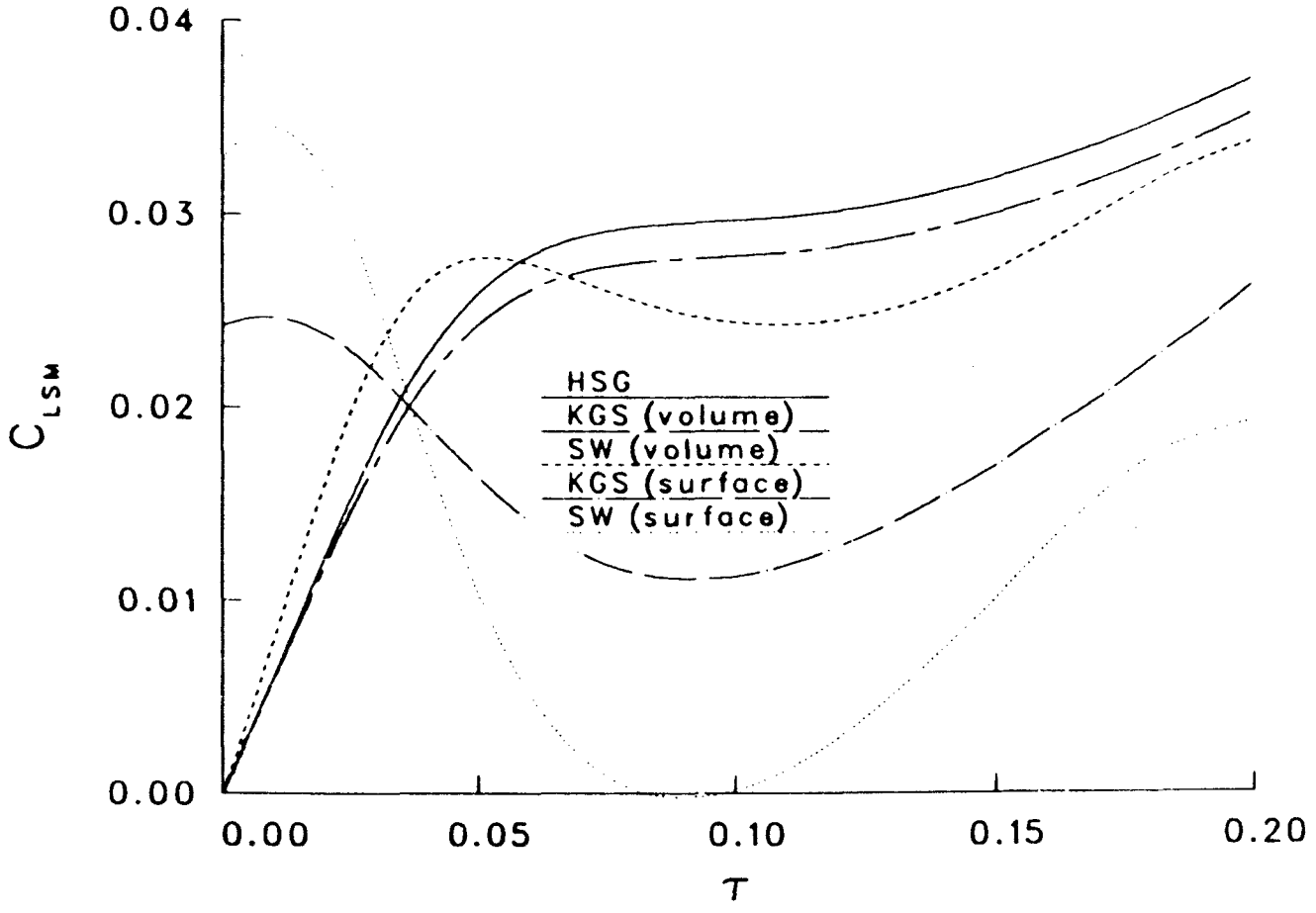

Fig. 3. C_{LSM} (by KGS and SW, volume and surface methods) vs. τ (Re = 500, A = 3).

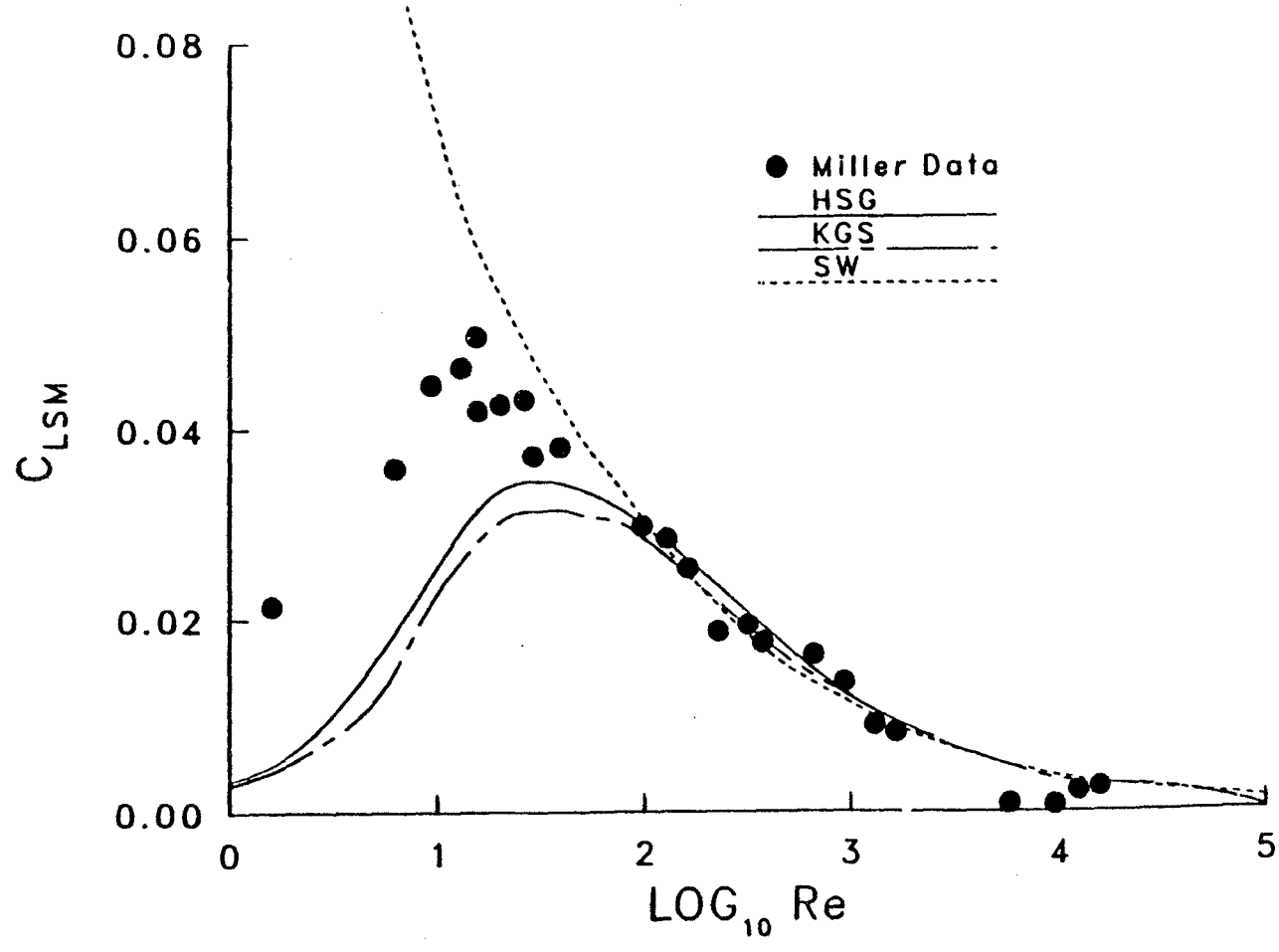

Fig. 4. C_{LSM} vs. $\log_{10}$ Re
for A = 4.5, τ = 0.1. Comparison with Miller data.

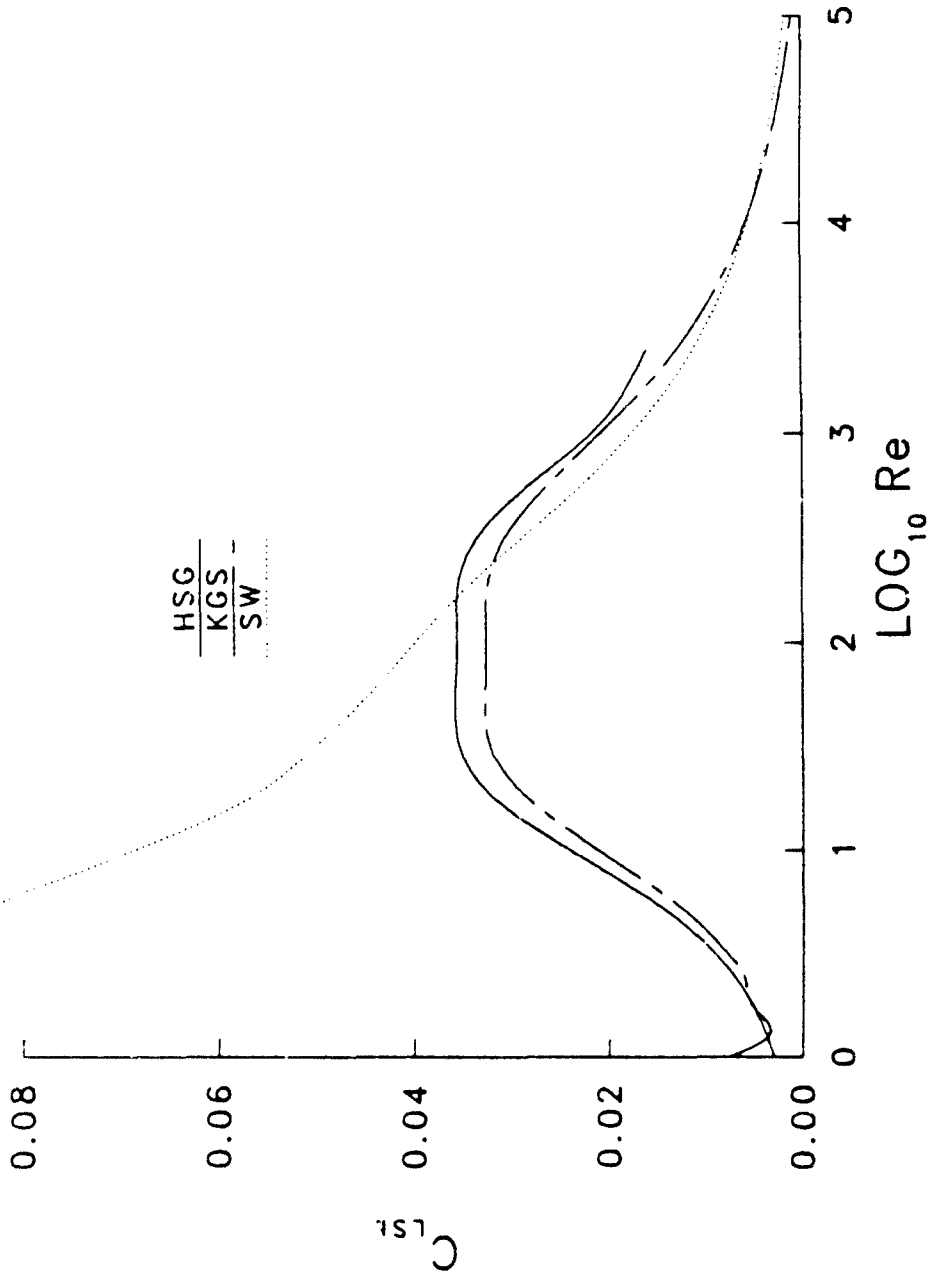

Fig. 5 C_{LSM} vs. $\log_{10}$ Re
for $A = 3$, $\tau = 0.1$

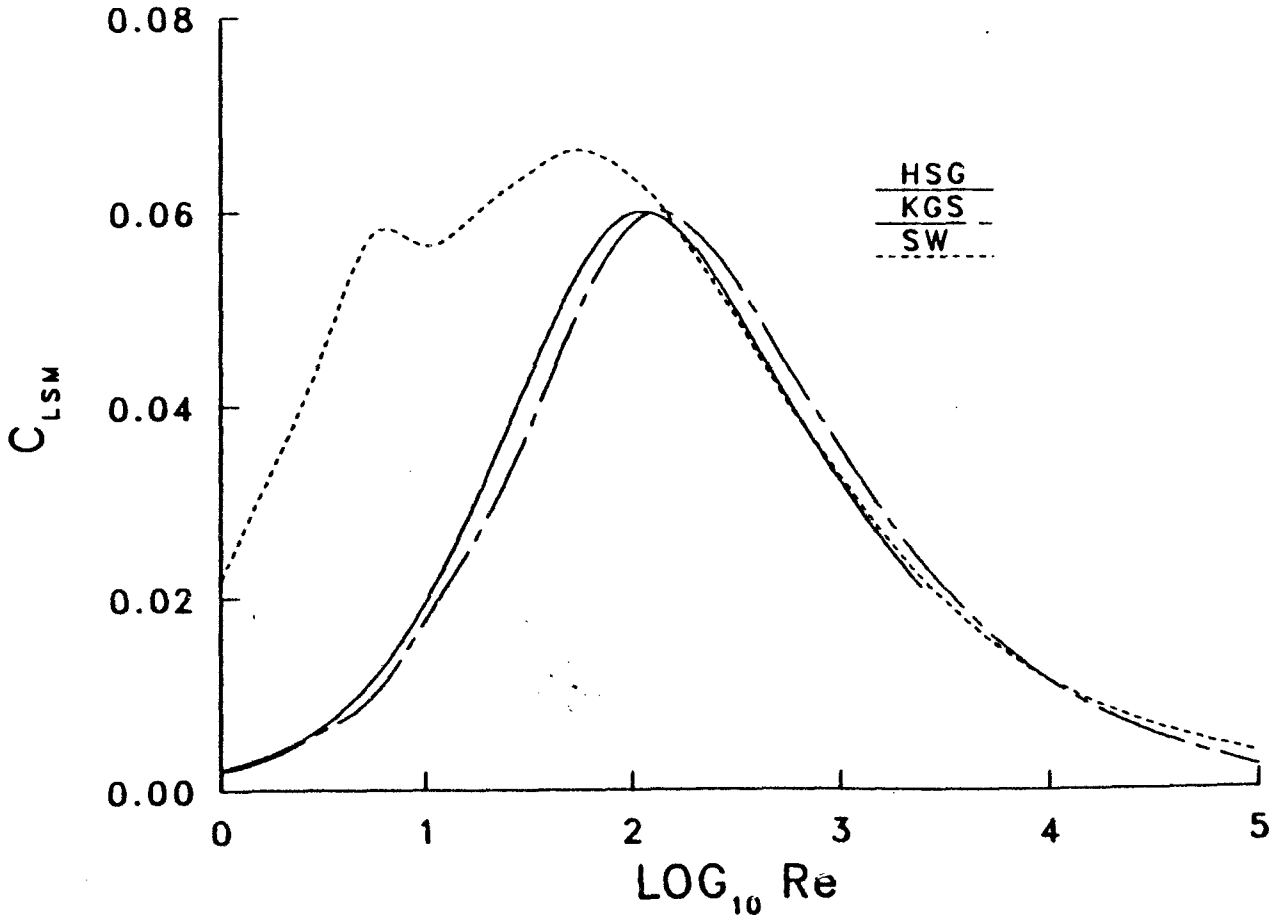

Fig. 6. C_{LSM} vs. $\log_{10}$ Re for A = 1.5, τ = 0.1

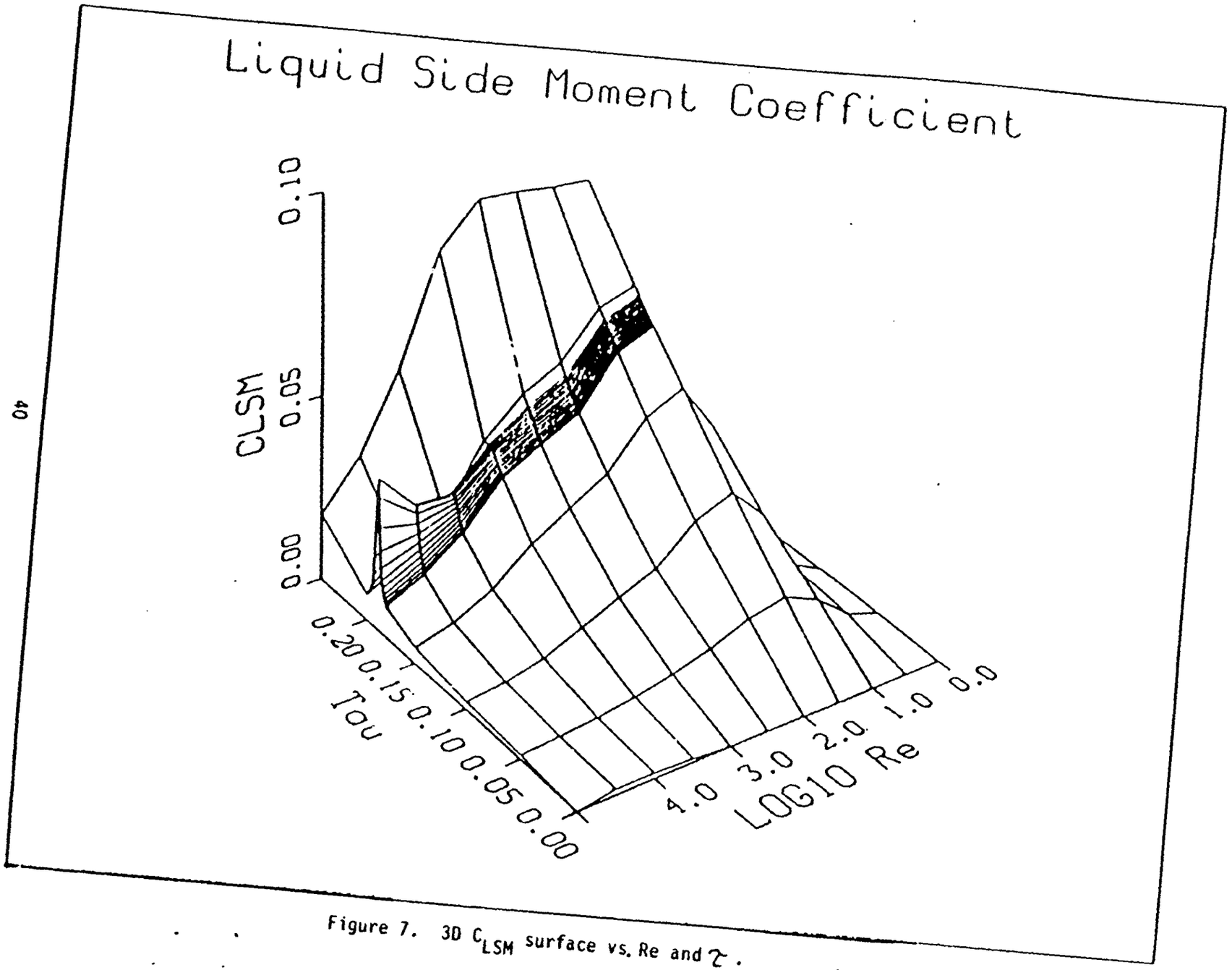

Figure 7. 3D C_{LSM} surface vs. Re and τ.

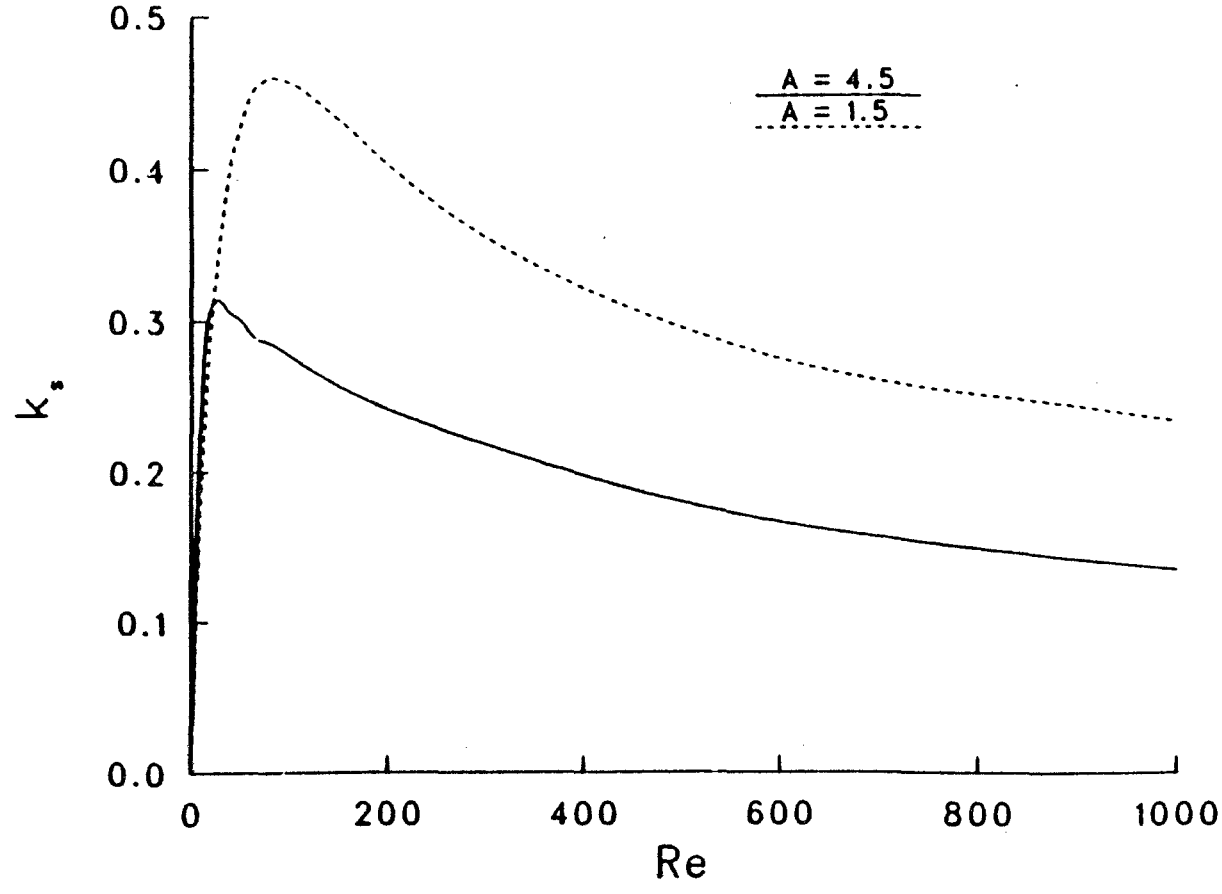

Fig. 8. k_s vs. Re for A = 1.5 and 4.5.

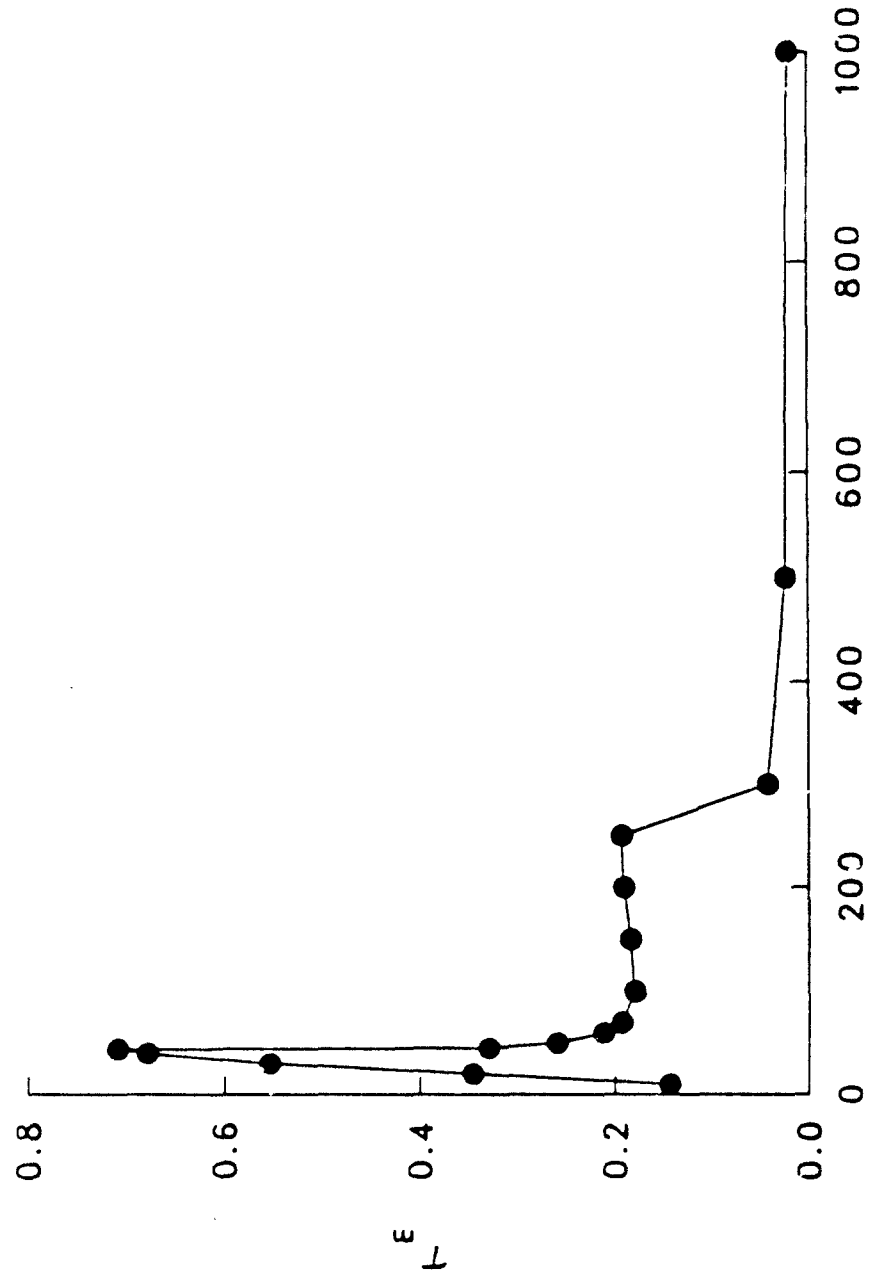

Figure 9. τ_m vs. Re for A = 1.5

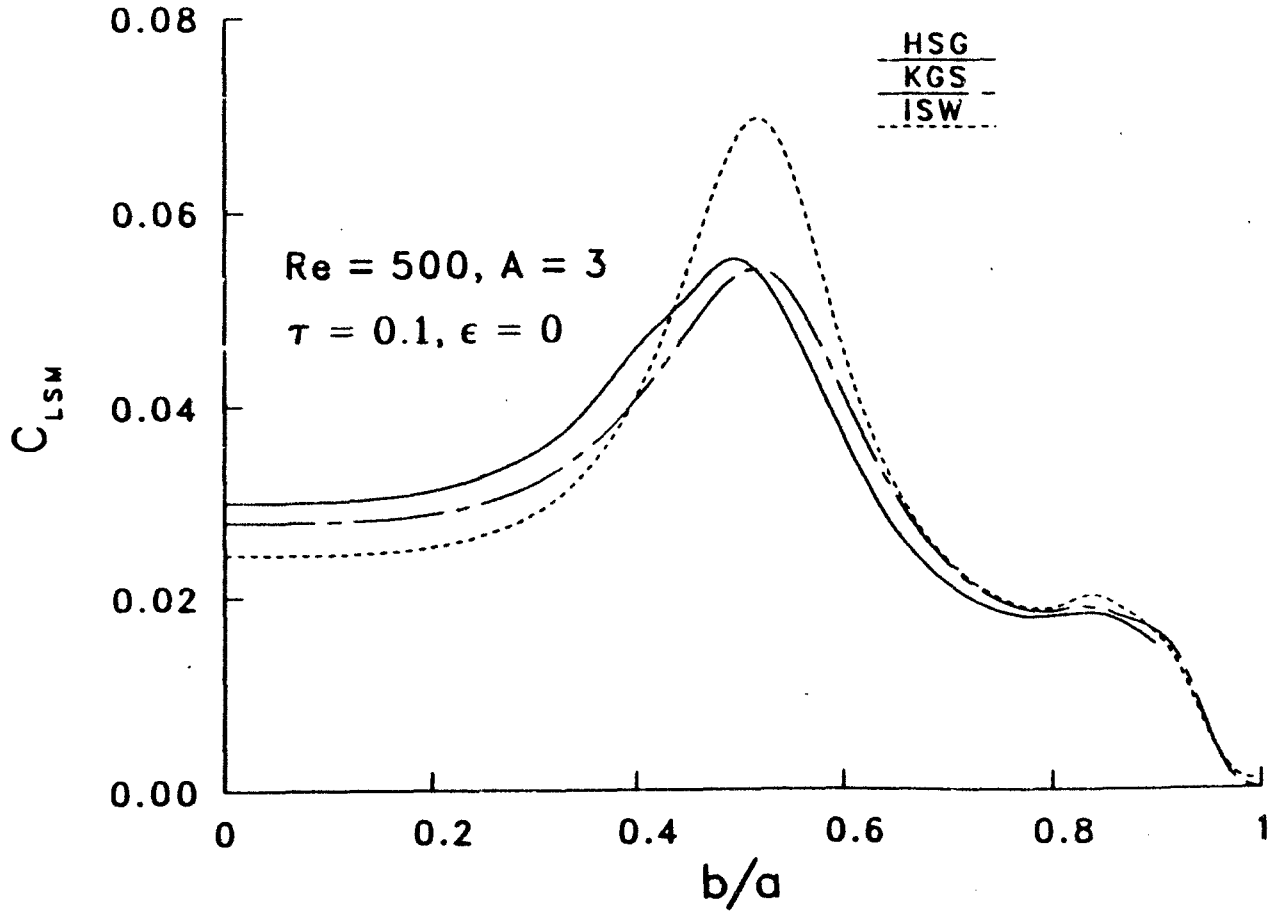

Fig. 10 Partial Fill: C_{LSM} vs. b/a

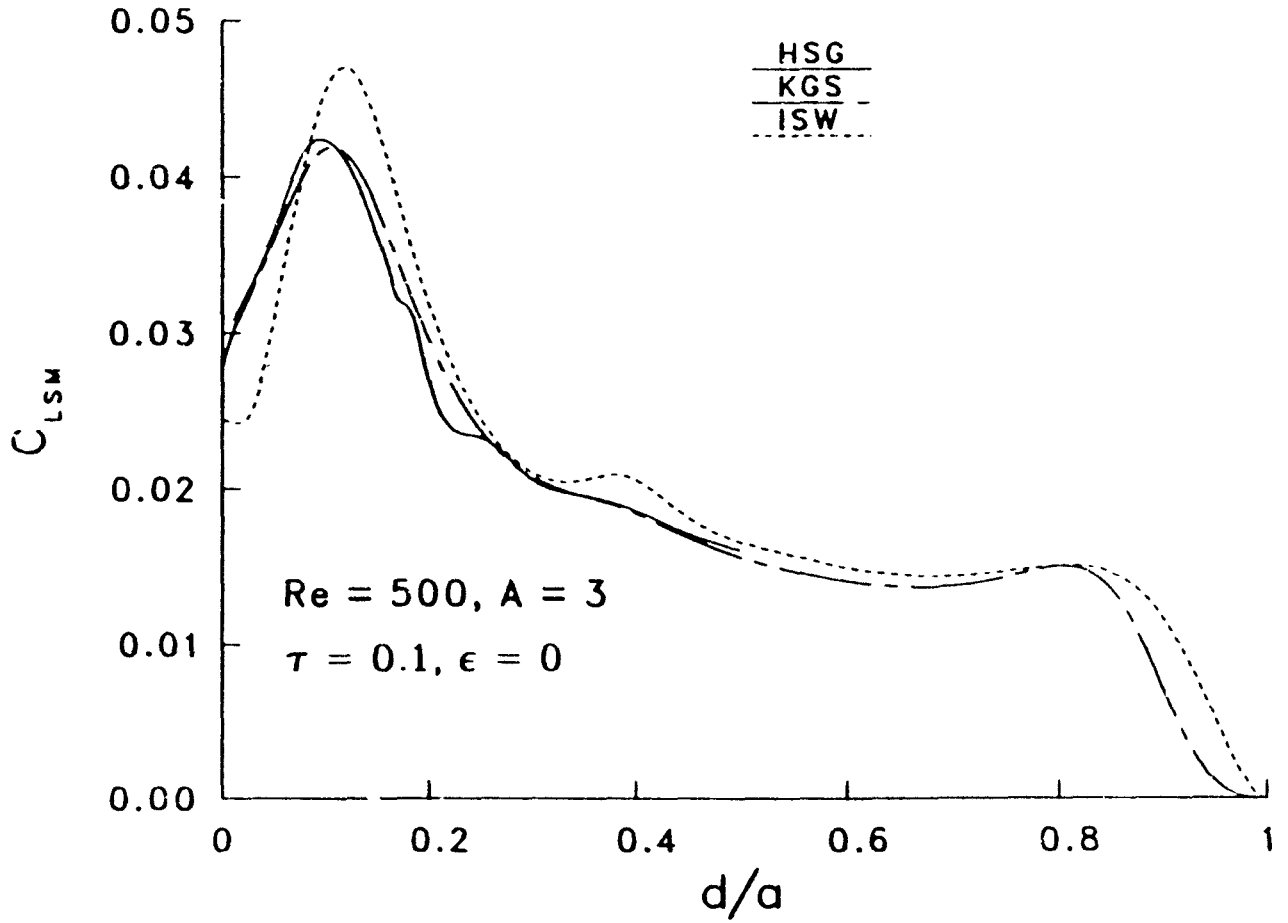

Fig. 11 Central Rod: C_{LSM} vs. d/a

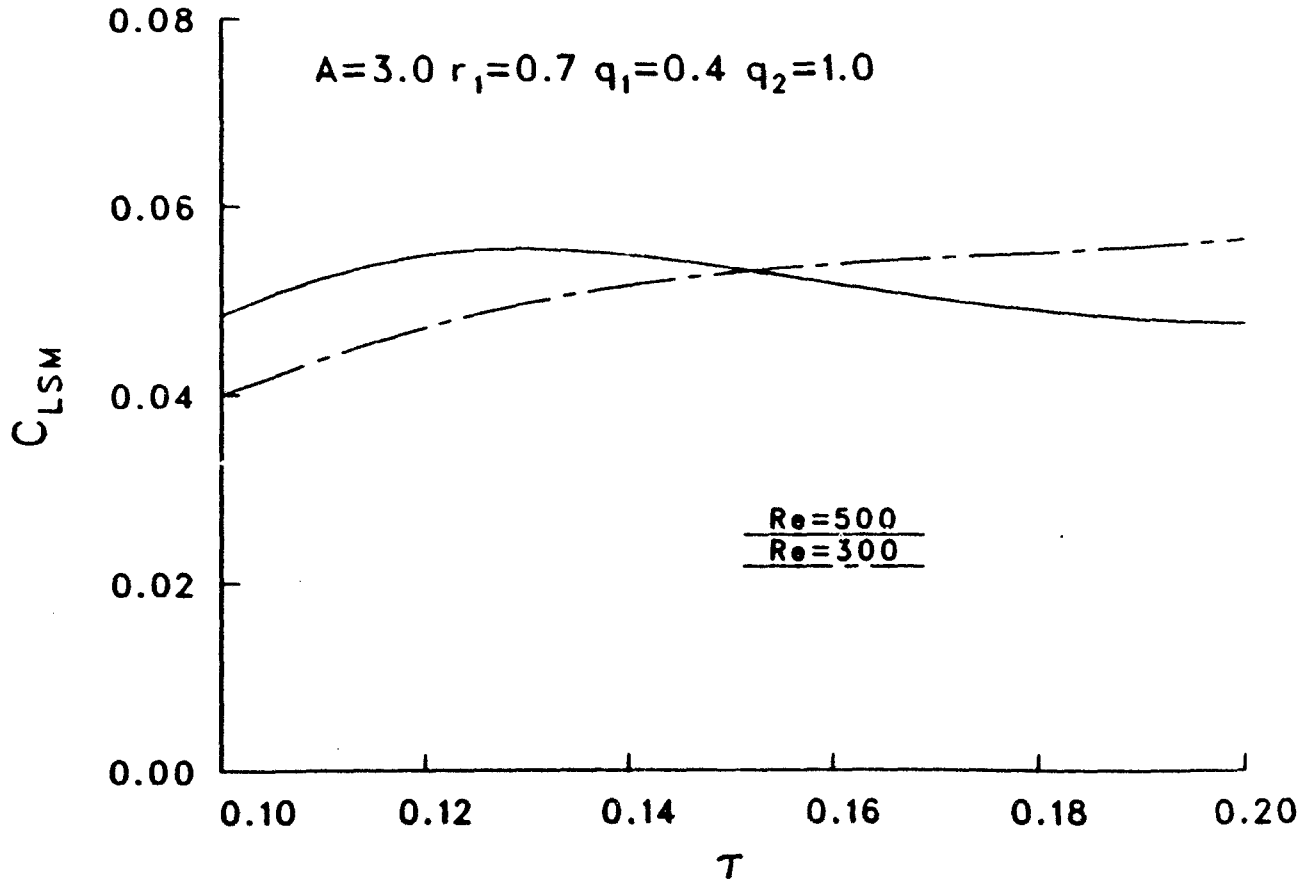

Figure 12. Binary: C_{LSM} vs. τ.

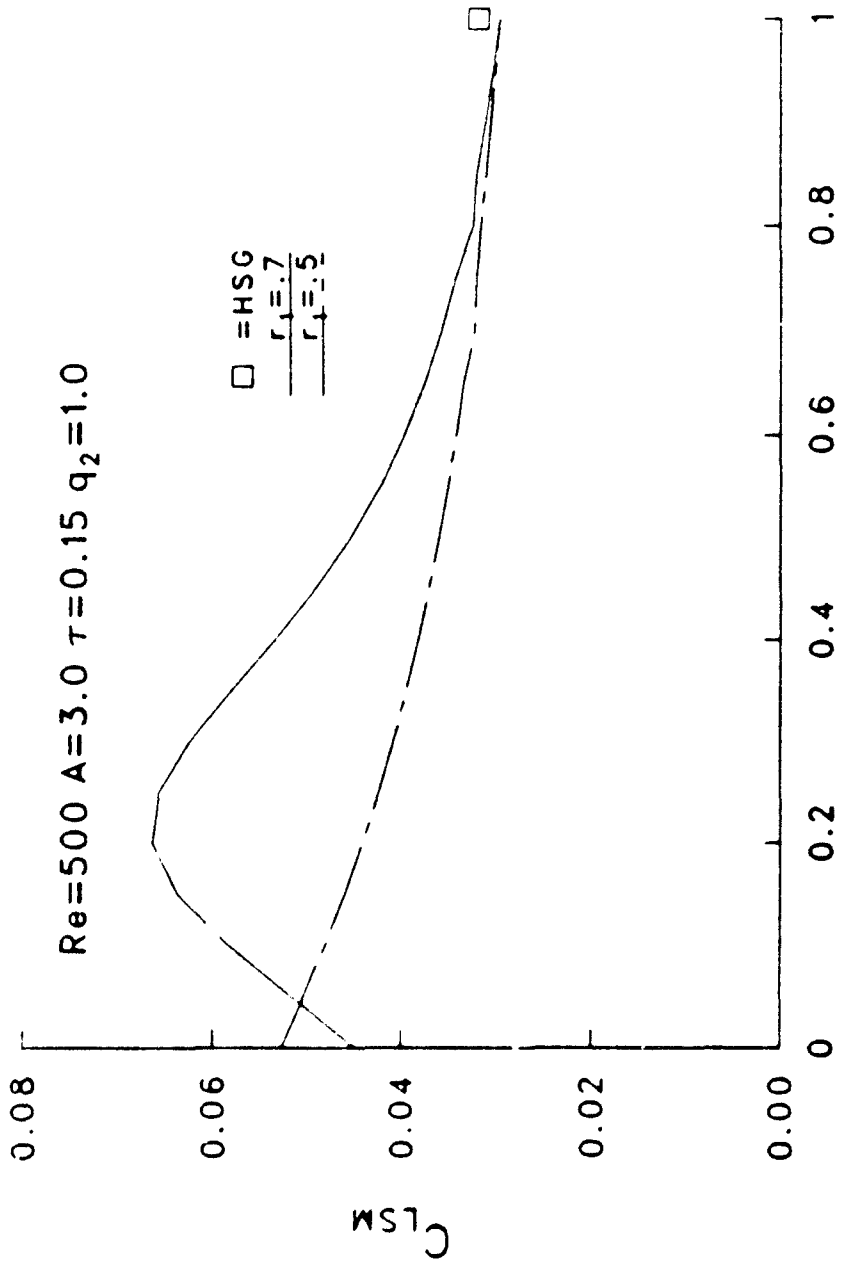

Figure 13. Binary: C_{LSM} vs. q_1.

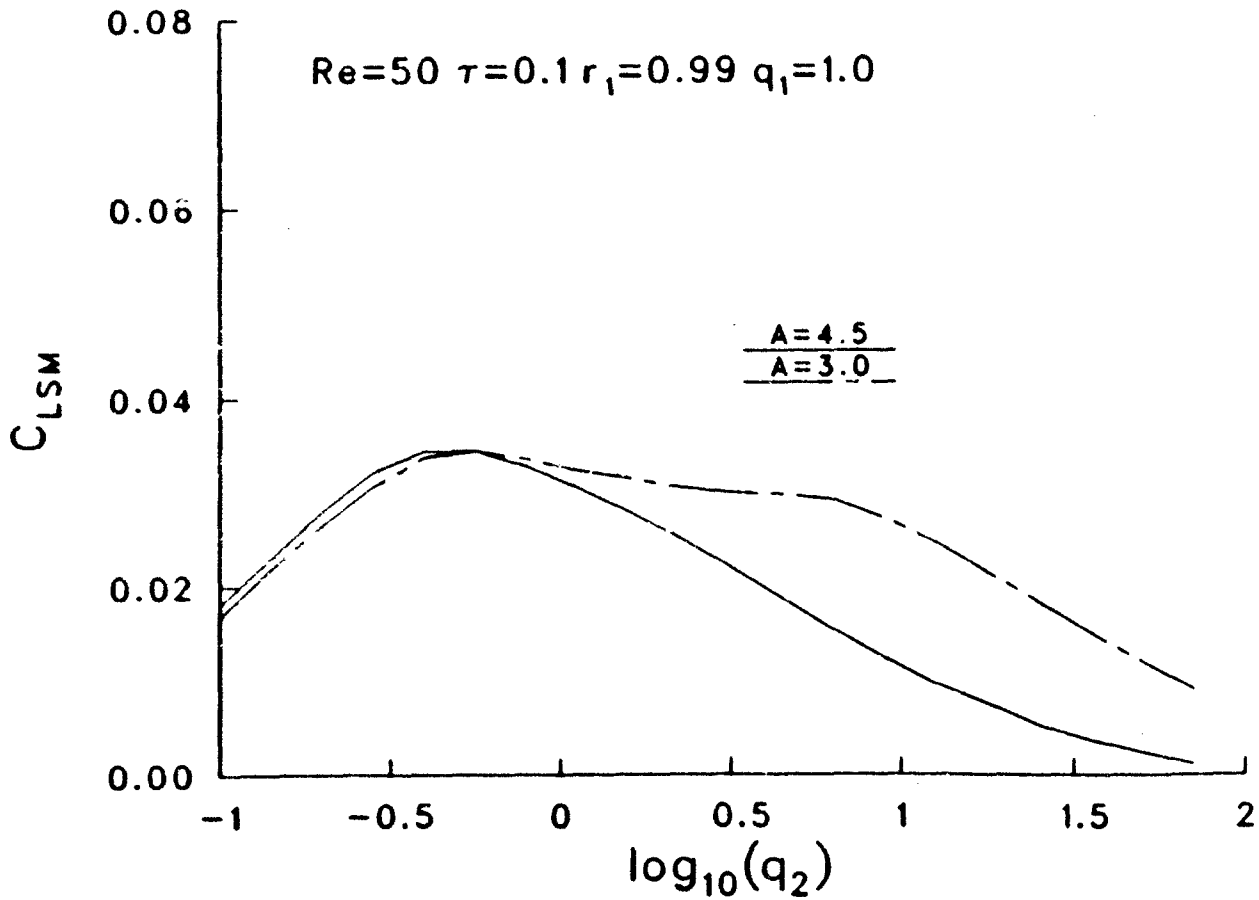

Figure 14. Binary: C_{LSM} vs. $\log_{10}(q_2)$.

INTENTIONALLY LEFT BLANK.

References

[1] Stewartson, K., "On the Stability of a Spinning Top Containing Liquid," *Journal of Fluid Mechanics*, Vol. 5, Part 4, September 1959, pp. 577-592.

[2] Wedemeyer, E.H., "Viscous Corrections to Stewartson's Stability Criterion," US Army Ballistic Research Laboratory (Aberdeen Proving Ground, MD) Report BRL-R-1325, June 1966. (AD 489687)

[3] Frasier, J.T., "Dynamics of a Liquid Filled Shell: Viscous Effects in a Cylindrical Cavity with a Central Rod," US Army Ballistic Research Laboratory (Aberdeen Proving Ground, MD) Memorandum Report BRL-MR-1959, January 1969. (AD 684344)

[4] Murphy, C.H., "Angular Motion of a Spinning Projectile with a Viscous Liquid Payload," *Journal of Guidance, Control, and Dynamics*, Vol. 6, July-August 1983, pp. 280-286. [See also US Army Ballistic Research Laboratory (Aberdeen Proving Ground, MD) Memorandum Report ARBRL-MR-03194, August 1982. (AD A118676)]

[5] Sedney, R. and Gerber, N., "Viscous Effects in the Wedemeyer Model of Spin-Up from Rest," US Army Ballistic Research Laboratory (Aberdeen Proving Ground, MD) Technical Report ARBRL-TR-02493, June 1983. (AD A129506)

[6] Murphy, C.H., "Moment Induced by a Liquid Payload During Spin-Up Without a Critical Layer," *Journal of Guidance, Control, and Dynamics*, Vol. 8, May-June 1985. [See also US Army Ballistic Research Laboratory (Aberdeen Proving Ground, MD) Technical Report ARBRL-TR-02581, August 1984. (AD A145716)]

[7] Murphy, C.H., "Side Moment Exerted by a Two-Component Liquid Payload on a Spinning Projectile," *Journal of Guidance, Control, and Dynamics*, Vol. 10, January-February 1987. [See also US Army Ballistic Research Laboratory (Aberdeen Proving Ground, MD) Technical Report ARBRL-TR-02624, December 1984. (AD A149845)]

[8] Murphy, C.H., "Moment Exerted on a Coning Projectile by a Spinning Liquid in a Spheroidal Cavity," *AIAA Journal*, Vol. 6, December 1987, pp. 1631-1633. [See also US Army Ballistic Research Laboratory (Aberdeen Proving Ground, MD) Technical Report ARBRL-TR-02755, December 1986. (AD A177642)]

[9] Murphy, C.H., "Liquid Payload Roll Moment Induced by a Spinning and Coning Projectile," *AIAA* Paper No. 83-2142, *AIAA* Atmospheric Flight Mechanics Conference, August 1983. [See also US Army Ballistic Research Laboratory (Aberdeen Proving Ground, MD) Technical Report ARBRL-TR-02521, September 1983. (AD 133681)]

[10] Kitchens, C.W., Jr., Gerber, N., and Sedney, R., "Oscillations of a Liquid in a Rotating Cylinder: Part I. Solid Body Rotation," US Army Ballistic Research Laboratory (Aberdeen Proving Ground, MD) Technical Report ARBRL-TR-02081, June 1978. (AD A057759)

[11] Gerber, N., Sedney, R., and Bartos, J., "Pressure Moment on a Liquid-Filled Projectile: Solid Body Rotation," US Army Ballistic Research Laboratory (Aberdeen Proving Ground, MD) Technical Report ARBRL-TR-02422, October 1982. (AD A120567)

[12] Gerber, N. and Sedney, R., "Moment on a Liquid-Filled Spinning and Nutating Projectile: Solid Body Rotation," US Army Ballistic Research Laboratory (Aberdeen Proving Ground, MD) Technical Report ARBRL-TR-02470, February 1983. (AD A125332)

[13] Gerber, N., "Contribution of Pressure to the Moment During Spin-Up on a Nutating Liquid-Filled Cylinder: Ad Hoc Model," US Army Ballistic Research Laboratory (Aberdeen Proving Ground, MD) Technical Report ARBRL-TR-02563, June 1984. (AD A143678)]

[14] Gerber, N., "Liquid Moment on a Filled Coning Cylinder During Spin-Up: Ad Hoc Model," US Army Ballistic Research Laboratory (Aberdeen Proving Ground, MD) Technical Report ARBRL-TR-02628, December 1984. (AD A150280)

[15] Vaughn, H.R., Oberkampf, W., and Wolfe, W.R., "Fluid Motion Inside a Spinning Nutating Cylinder," *Journal of Fluid Mechanics*, Vol. 150, 1985, pp. 121-138.

[16] Strikwerda, J.C. and Nagel, Y.M., "A Numerical Method for Computing the Flow in Rotating and Coning Fluid-Filled Cylinders," Paper No. CRDC-SP-85006, Conference on Chemical Defense Research, Aberdeen Proving Ground, MD, 1984 .

[17] Strikwerda, J.C. and Nagel, Y.M., "A Numerical Method for the Incompressible Navier-Stokes Equations in Three-Dimensional Cylindrical Geometry," *Journal of Computational Physics* 78, 1988, pp.64-78.

[18] Rosenblat, S., Gooding, A. and Engleman, M.S., "Finite Element Calculations of Viscoelastic Fluid Flow in a Spinning and Nutating Cylinder," U.S. Army Chemical Research, Development and Engineering Center, Aberdeen Proving Ground, MD, Report CRDEC-CR-87021, December 1986.

[19] Herbert, Thorwald, "Viscous Fluid Motion in a Spinning and Nutating Cylinder," Chemical Research and Development Center, Aberdeen Proving Ground, MD, Report CRDC-CR-86004, November 1985.

[20] Herbert, Th., and Li, R., "Numerical Study of the Flow in a Spinning and Nutating Cylinder," *AIAA* Paper No. 87-1445, *AIAA* 19th Fluid Dynamics, Plasma Dynamics and Laser Conference, June 1987.

[21] Hall, P., Sedney, R., and Gerber, N., "Fluid Motion in a Spinning, Coning Cylinder via Spatial Eigenfunction Expansion," US Army Ballistic Research Laboratory (Aberdeen Proving Ground, MD) Technical Report BRL-TR-02813, August 1987. (AD A190758)

[22] Nusca, M.J., "Computational Fluid Dynamics Methods for Low Reynolds Number Processing/Spinning Incompressible Flows," US Army Ballistic Research Laboratory (Aberdeen Proving Ground, MD) Memorandum Report BRL-MR-03657, April 1988. (AD A193891)

[23] Murphy, C.H., "Free Flight Motion of Symmetric Missiles," US Army Ballistic Research Laboratory (Aberdeen Proving Ground, MD) Report R1216, July 1963. (AD 442757)

[24] D'Amico, W.P., Beims, W.G., and Rogers, T.H., "Pressure Measurements of a Rotating Liquid for Impulsive Coning Motion," US Army Ballistic Research Laboratory (Aberdeen Proving Ground, MD) Memorandum Report BRL-MR-03208. (AD 121603) (See also *AIAA* Paper 82-0249, January 1982.)

[25] Sedney, Raymond and Gerber, Nathan, "Asymptotic Analysis of the Roots of a Certain Transcendental Equation," US Army Ballistic Research Laboratory (Aberdeen Proving Ground, MD) Technical Report TR-2727, April 1986. (AD A168315)

[26] Scott, M.R. and Watts, H.A., "SUPORT - A Computer Code for Two-Point Boundary-Value Problems via Orthonormalization," Sandia Laboratories (Albuquerque, NM) Report SAND75-0198, June 1975.

[27] Scheid, Francis, *Theory and Problems of Numerical Analysis*, Schaum's Outline Series, McGraw-Hill Book Co., New York, 1968.

[28] Scott, Wayman E., "The Inertial Wave Frequency Spectrum in a Cylindrically Confined, Inviscid, Incompressible, Two Component Liquid," US Army Ballistic Research Laboratory (Aberdeen Proving Ground, MD) Technical Report R-1609, September 1972. (AD 752439) (See also *Physics of Fluids*, Vol.16, No.1, pp.9-12, January 1973.)

[29] Gans, Roger F., "Dynamics of a Near-Resonant Fluid-Filled Gyroscope," *AIAA Journal*, Vol.22, No.10, October 1984, pp.1465-1471.

[30] Miller, Miles C., "Flight Instabilities of Spinning Projectiles Having Non-Rigid Payloads," *Journal of Guidance, Control and Dynamics*, Vol. 5, March-April 1982, pp.151-157.

[31] D'Amico, W.P. and Miller, M.C., "Flight Instability Produced by a Rapidly Spinning, Highly Viscous Liquid," *Journal of Spacecraft and Rockets*, Vol. 16, January-February 1979, pp.62-64.

[32] Miller, Miles C., "Liquid Filled Projectiles - New problems, New Solutions," *Proceedings of the 9th International Symposium on Ballistics*, American Defense Preparedness Association, Shrivenham, England, 29-30 April, 1 May 1986, pp. 2-67 to 2-76.

[33] Miller, Miles C., "Laboratory Test Fixture for Non-Rigid Payloads," *Proceedings of the 13th International Congress on Instrumentation in Aerospace Simulation Facilities* Göttingen, FRG, 18-21 September 1989.

[34] Kayser, Lyle D., D'Amico, William P.,Jr. and Brannan, William I., "Free Gyroscope Experiment of Two Immiscible Liquids in a Partially-Filled Container," US Army Ballistic Research Laboratory (Aberdeen Proving Ground, MD) Memorandum Report MR-3484, December 1985. (AD A164937) [See also: AIAA-85-1823, AIAA 12th Atmospheric Flight Mechanics Conference, August 19-21, 1985, Snowmass, Colorado.]

INTENTIONALLY LEFT BLANK.

Appendix A: Effect of Center-of-Mass Axial Offset

If the projectile's center of mass is not at the center of the cylinder, the liquid moment should be computed relative to the projectile's center of mass. Since the projectile's coning motion is relative to its center of mass, the boundary conditions on the liquid are also changed. In this appendix, we will consider both of these effects.

We will locate the projectile's center of mass relative to the center of the cylinder by the dimensionless distance $L = h/a$. This distance will be negative if the projectile center of mass is to the rear of the cylinder center. Eqs.(10-12) become

$$x - L = \tilde{x} - L + \tilde{r}R\{Ke^{-i\tilde{\psi}}\} \quad (A1)$$

$$r = \tilde{r} - (\tilde{x} - L)R\{Ke^{-i\tilde{\psi}}\} \quad (A2)$$

$$\tilde{\psi} - \psi = -\left(\frac{\tilde{x} - L}{\tilde{r}}\right) R\{iKe^{-i\tilde{\psi}}\} \quad (A3)$$

The new boundary conditions become:

(a) on the cylindrical wall ($\tilde{r} = 1$):

$$\underline{w}(1, x) = i(1 - f) \quad (A4)$$

$$\underline{u}(1, x) = -i(1 - f)(x - L) \quad (A5)$$

$$\underline{v}(1, x) = -(1 - f)(x - L) \quad (A6)$$

(b) on the end-walls ($\tilde{x} \pm A$):

$$\underline{w}(r, \pm A) = i(1 - f)r \quad (A7)$$

$$\underline{u}(r, \pm A) = i(1 - f)(\mp A - L) \quad (A8)$$

$$\underline{v}(r, \pm A) = (1 - f)(\mp A - L) \quad (A9)$$

If we add a subscript 'c' to $\underline{w}, \underline{u}, \underline{v}, \underline{p}$ and C_p to denote those variables for L = 0, then more general variables can be defined by the relations:

$$\underline{w} = \underline{w}_c + Lf\left[xZ_{4L}(r) + \sum_{k=1}^{N} c_{Lk}Z_{4k}(r)G_k(x)\right] \quad (A10)$$

$$\underline{u} = \underline{u}_c + L\left[i(1 - f) + fZ_{1L}(r) + f\sum_{k=1}^{N} c_{Lk}Z_{1k}(r)H_k(x)\right] \quad (A11)$$

$$\underline{u} - i\underline{v} = \underline{u}_c - i\underline{v}_c + Lf\left[Z_{2L}(r) + \sum_{k=1}^{N} c_{Lk}Z_{2k}(r)H_k(x)\right] \quad (A12)$$

$$\underline{p} = \underline{p}_c + L\left[(1 - f^2)r + fZ_{6L}(r) + f\sum_{k=1}^{N} c_{Lk}Z_{6k}(r)H_k(x)\right] \quad (A13)$$

$$C_p = C_{p_c} + Lf\left[-fr + Z_{6L}(r) + \sum_{k=1}^{N} c_{Lk}Z_{6k}(r)H_k(x)\right] \quad (A14)$$

The terms involving Z_{jL} must satisfy the linear Navier-Stokes equations. This means that they are solutions of Eqs.(52-57) when index k is replaced by the symbol L in each subscript and when

$$\lambda_L = 0, \quad \lambda_{L1} = 1, \quad \lambda_{L2} = 0 \tag{A15}$$

It can easily be seen that the other terms multiplied by L and outside the summation are also solutions of Eqs.(52-57) with k replaced by L.

We now require that the terms multiplied by L satisfy the boundary conditions multiplied by L. For $\tilde{r} = 1$,

$$Z_{1L}(1) = Z_{2L}(1) = Z_{4L}(1) = 0 \tag{A16}$$

For the interior boundary conditions:

(a) for a fully-filled cylinder:

$$Z_{6L}(0) = Z_{2L}(0) = Z_{4L}(0) = 0 \tag{A17}$$

(b) for a partially-filled cylinder:

$$Z_{6L}(r_0) + \frac{ir_0 Z_{1L}(r_0)}{1-f} - \frac{2Z'_{1L}(r_0)}{Re} = fr_0 \tag{A18}$$

$$Z_{5L}(r_0) = 0 \tag{A19}$$

$$r_0 Z_{3L}(r_0) - iZ_{2L}(r_0) = 0 \tag{A20}$$

(c) for a cylinder with a central rod:

$$Z_{1L}(r_0) = Z_{2L}(r_0) = Z_{4L}(r_0) = 0 \tag{A21}$$

Note that Eqs.(55-56) contain only Z_{4L} and Z_{5L}. Since the boundary conditions for these variables are homogeneous,

$$Z_{4L}(r) \equiv Z_{5L}(r) \equiv 0 \tag{A22}$$

On the end-walls:

$$\sum_{k=1}^{N} c_{Lk} Z_{4k}(r) = 0 \tag{A23}$$

$$Z_{1L}(r) + \sum_{k=1}^{N} c_{Lk} h_k Z_{1k}(r) = 0 \tag{A24}$$

$$Z_{2L}(r) + \sum_{k=1}^{N} c_{Lk} h_k Z_{2k}(r) = 0 \tag{A25}$$

For the fully filled and central rod cases, all the boundary conditions are homogeneous and therefore

$$Z_{jL}(r) \equiv 0 \tag{A26}$$

For these cases, Eqs.(A23-A25) can be satisfied by

$$c_{Lk} = 0 \qquad (A27)$$

and only the pressure components of the liquid moment are affected. If moments are computed with respect to the actual center of mass, the entries for C_{mpl} and C_{mpr} in Table 4 must be modified by the following increments:

$$\Delta C_{mpl} = -i(1 - i\epsilon) f L^2 \qquad (A28)$$

$$\Delta C_{mpr} = i r_0^2 (1 - i\epsilon) f L^2 \qquad (A29)$$

For the partially-filled case, however, the presence of the free surface makes the situation much more complicated. Four of the entries in Table 4 must be modified; the required increments are given in Table 8.

INTENTIONALLY LEFT BLANK.

Appendix B: Linear Moment from Angular Momentum

If we apply Eqs.(10-12,19-21) to the definitions of the N_j's (Table 6), we obtain the following linear expansions:

$$N_1 = a\dot{\phi}[\tilde{r}^2 + Kg_1] \qquad (B1)$$

$$N_2 = -a\dot{\phi}\left[\tilde{r}\dot{x}\cos\tilde{\psi} + (K/2)R\{i\tilde{N} + g_2\}\right] \qquad (B2)$$

$$N_3 = -a\dot{\phi}\left[\tilde{r}\tilde{x}\sin\tilde{\psi} + (K/2)R\{\tilde{N} + g_3\}\right] \qquad (B3)$$

where

$$\tilde{N} = \tilde{r}(i\tilde{r} - \underline{w}) + \tilde{x}(\underline{u} + i\underline{v} + 2i\tilde{x})$$

$$g_j = g_j(\tilde{r}, \tilde{x}, \tilde{\psi})$$

$$\int_0^{2\pi} g_j\, d\tilde{\psi} = 0$$

Since

$$\rho(\tilde{r}) = 0, \quad 0 < \tilde{r} < \tilde{r}_f(\tilde{x}, \tilde{\psi})$$

$$= \rho_2, \quad \tilde{r}_f(\tilde{x}, \tilde{\psi}) < \tilde{r} < \tilde{r}_i(\tilde{x}, \tilde{\psi})$$

$$= \rho_1, \quad \tilde{r}_i(\tilde{x}, \tilde{\psi}) < \tilde{r} \leq 1$$

we can write

$$\rho_1^{-1}\int_0^1\int_{-A}^{A}\int_0^{2\pi} \rho N_j \tilde{r}\, d\tilde{\psi}\, d\tilde{x}\, d\tilde{r} = M_{1j} + q_1 M_{2j} + q_1 M_{3j} + M_{4j} \qquad (B4)$$

where

$$M_{1j} = \int_{r_0}^1\int_{-A}^{A}\int_0^{2\pi} q_{1r} N_j \tilde{r}\, d\tilde{\psi}\, d\tilde{x}\, d\tilde{r}$$

$$M_{2j}, M_{3j}, M_{4j} = \int_{-A}^{A}\int_0^{2\pi}\int_{r_A}^{r_B} N_j \tilde{r}\, d\tilde{r}\, d\tilde{\psi}\, d\tilde{x}$$

$$(r_A, r_B) = (\tilde{r}_f, \tilde{r}_0)\ for\ M_{2j}$$

$$= (\tilde{r}_1, \tilde{r}_i)\ for\ M_{3j}$$

$$= (\tilde{r}_i, \tilde{r}_1)\ for\ M_{4j}$$

For a central rod, $\tilde{r}_f = \tilde{r}_0$ and $M_{2j} = 0$. Linear expansions of the M_{ij}'s yield

$$L_1 = 2m_L a^2 \dot{\phi} B_1 \qquad (B5)$$

$$L_2 = m_L a^2 \dot{\phi} K R\{iS\} \qquad (B6)$$

$$L_3 = m_L a^2 \dot{\phi} K R\{S\} \qquad (B7)$$

where

$$S = I + (1 - q_1) f F_2(r_1) + q_1 q_4 f F_2(r_0)$$

$$I = -(1/2A)\int_{r_0}^1\int_{-A}^{A} q_{1r}\tilde{N}\tilde{r}\, d\tilde{x} d\tilde{r}$$

$$fF_2(r) = -\frac{r^2}{2(1-f)A}\int_{-A}^{A}[\underline{u}(r, \tilde{x}) + i(1-f)\tilde{x}]\tilde{x}\, d\tilde{x}$$

and where $q_4 = 1$ for the partially filled case and zero otherwise.

Note from the definition of $\tilde{N}$ that the M_{ij}'s involve the volume integral V_1 of $\tilde{r}(i\tilde{r} - \underline{w})$ and the volume integral V_2 of $\tilde{x}(\underline{u} + i\underline{v} + 2i\tilde{x})$. We now derive a relation between V_1 and V_2 in order to eliminate V_2. The continuity equation for the perturbation velocity functions is[10,11]:

$$C \equiv \frac{\partial(\tilde{r}\underline{u})}{\partial\tilde{r}} - i\underline{v} + \tilde{r}\frac{\partial\underline{w}}{\partial\tilde{x}} = 0 \qquad (B8)$$

If we integrate by parts the volume integral of $q_{1r}\tilde{r}\tilde{x}C$, we obtain

$$\int_{-A}^{A}\left\{\left[\tilde{r}^2\underline{u}\right]_{r_1}^{1} + \left[q_1\tilde{r}^2\underline{u}\right]_{r_0}^{r_1}\right\}\tilde{x}\,d\tilde{x} + \int_{r_0}^{1} q_{1r}\left[\tilde{x}\underline{w}\right]_{-A}^{A}\tilde{r}^2\,d\tilde{r}$$
$$- \int_{r_0}^{1}\int_{-A}^{A} q_{1r}[(\underline{u} + i\underline{v})\tilde{x} + \underline{w}\tilde{r}]\tilde{r}\,d\tilde{x}\,d\tilde{r} = 0 \qquad (B9)$$

Adding $i\tilde{x}$ and $i\tilde{r}$ terms as needed to obtain the desired expressions, we have

$$\int_{-A}^{A}\left\{\left[\tilde{r}^2(\underline{u} + i\tilde{x})\right]_{r_1}^{1} + \left[q_1\tilde{r}^2(\underline{u} + i\tilde{x})\right]_{r_0}^{r_1}\right\}\tilde{x}\,d\tilde{x} + \int_{r_0}^{1} q_{1r}\left[\tilde{x}(\underline{w} - i\tilde{r})\right]_{-A}^{A}\tilde{r}^2\,d\tilde{r}$$
$$- \int_{r_0}^{1}\int_{-A}^{A} q_{1r}[(\underline{u} + i\underline{v} + 2i\tilde{x})\tilde{x} + (\underline{w} - i\tilde{r})\tilde{r}]\tilde{r}\,d\tilde{x}\,d\tilde{r} = 0 \qquad (B10)$$

which reduces to the desired relation:

$$(1/2A)\int_{r_0}^{1}\int_{-A}^{A} q_{1r}(\underline{u} + i\underline{v} + 2i\tilde{x})\tilde{x}\tilde{r}\,d\tilde{x}\,d\tilde{r} = (1/2A)\int_{r_0}^{1}\int_{-A}^{A} q_{1r}(i\tilde{r} - \underline{w})\tilde{r}^2\,d\tilde{x}\,d\tilde{r}$$
$$+(1-f)f[q_1F_2(r_0) + (1-q_1)F_2(r_1) - F_2(1)]$$
$$+ifB_2(2A^2/3) - ifB_1 - fG \qquad (B11)$$

where

$$F_2(r) = \frac{r^2}{2(1-f)}\left\{(2A^2/3)\left[\tilde{f} - c_0Z_{10}(r)\right] - (1/A)\sum c_kD_kZ_{1k}(r)\right\}$$
$$fG = \int_{r_0}^{1} q_{1r}[i(1-f)\tilde{r} - \underline{w}(\tilde{r}, A)]\tilde{r}^2\,d\tilde{r}$$

According to the boundary conditions, $F_2(1)$ and G are zero. This, of course, may not be the case for a finite number of eigenfunctions or for boundary layer solutions based on an approximate form of the continuity equation. However, $F_2(1) = 0$ is a valid assumption for HSG and HSGB. The actual nonzero value of $F_2(1)$ will be computed for the boundary layer theories. G will be computed exactly in all the theories.

Eq.(B11) can now be used to derive the formulas in Table 7.

Appendix C: End-Wall Boundary Layer Relations

The usual boundary layer assumptions can be made for the linearized Navier-Stokes equations [Eqs.(29-32)] in the vicinity of the end walls ($x = \pm A$). The subscript "be" will denote end-wall boundary layer functions.

$$\frac{\partial \underline{u}_{be}}{\partial r} + \underline{u}_{be} - i\underline{v}_{be} + r\frac{\partial \underline{w}_{be}}{\partial x} = 0 \qquad (C1)$$

$$i(f-1)\underline{u}_{be} - 2\underline{v}_{be} = \frac{1}{Re}\frac{\partial^2 \underline{u}_{be}}{\partial x^2} \qquad (C2)$$

$$i(f-1)\underline{v}_{be} + 2\underline{u}_{be} = \frac{1}{Re}\frac{\partial^2 \underline{v}_{be}}{\partial x^2} \qquad (C3)$$

$$\frac{\partial \underline{v}_{be}}{\partial x} = 0 \qquad (C4)$$

If the longitudinal symmetry of the boundary conditions is used, the solutions $\underline{u}_{be}$ and $\underline{v}_{be}$ to these equations take simple forms closely related to those given in References [4] and [12].

$$\underline{u}_{be} = (if/2)[-A(r)G_a(x) + B(r)G_b(x)] \qquad (C5)$$

$$\underline{v}_{be} = (f/2)[A(r)G_a(x) + B(r)G_b(x)] \qquad (C6)$$

where

$$G_a = \sin(i\alpha x)/\sin(i\alpha A)$$
$$G_b = \sin(i\beta x)/\sin(i\beta A)$$
$$\alpha = (1-i)[(3-f)Re/2]^{1/2}$$
$$\beta = (1+i)[(1+f)Re/2]^{1/2}$$

The functions $A(r)$ and $B(r)$ are determined by the no-slip conditions at $x = A$. If we denote the left sides of Eqs.(33-36) by $\hat{w}, \hat{u}, \hat{v}, \hat{p}$, we can write

$$\underline{u}(r,A) = (\hat{u} + \underline{u}_{be})_{x=A} = -i(1-f)A \qquad (C7)$$

$$\underline{v}(r,A) = (\hat{v} + \underline{v}_{be})_{x=A} = -(1-f)A \qquad (C8)$$

Thus

$$fA(r) = -(\hat{v} + i\hat{u})_{x=A} = -if\sum c_k Z_{2k}(r) \qquad (C9)$$

$$fB(r) = -[\hat{v} - i\hat{u} - 2(1-f)x]_{x=A}$$
$$= -if\{2\hat{f}A - \sum c_k[2Z_{1k}(r) - Z_{2k}(r)]\} \qquad (C10)$$

The continuity equation can now be used to obtain a relation for $\underline{w}_{be}$:

$$\underline{w}_{be} = \frac{-1}{2(1-f)}\left[\frac{(1+f)G_a(x)}{\alpha} + \frac{(3-f)G_b(x)}{\beta}\right]\frac{\partial \underline{w}(r,A)}{\partial x} \qquad (C11)$$

The boundary condition for the velocity normal to the end walls is

$$\underline{w}(r,\pm A) = (\hat{w} + \underline{w}_{be})_{x=\pm A} = i(1-f)r \qquad (C12)$$

or

$$\sum c_k Z_{4k}(r)[cos(\lambda_k A) + \lambda_k \delta_c \, sin(\lambda_k A)] = 0 \qquad (C13)$$

where

$$\begin{aligned} \delta_c &= \frac{-1}{2(1-f)}\left[\frac{1+f}{\alpha} + \frac{3-f}{\beta}\right] \\ &= \frac{-(1+i)}{2(1-f)\sqrt{2Re}}\left[\frac{1+f}{\sqrt{3-f}} + \frac{i(3-f)}{\sqrt{1+f}}\right] \end{aligned}$$

Thus λ_k must be selected so that

$$cos(\lambda_k A) + \lambda_k \delta_c \, sin(\lambda_k A) = 0 \qquad (C14)$$

The boundary condition for the normal velocity at the lateral wall is affected by the presence of the boundary layers at the end walls.

$$\underline{u}(1,x) = \hat{u}(1,x) + \underline{u}_{bc}(1,x) = -i(1-f)x \qquad (C15)$$

This reduces to

$$\sum c_k Z_{1k}(1) G_k(x) + (i/2)[-A(1)G_a(x) + B(1)G_b(x)] = \hat{f}x \qquad (C16)$$

Now

$$A(1) = 0 \qquad (C17)$$

$$B(1) = -2i\hat{f}(A - \sum a_k g_k) \qquad (C18)$$

where

$$g_k = G_k(A)$$

We select the Z_{1k}'s to be unity and the a_k's to be the least squares fit of

$$\sum a_k[G_k(x) - g_k G_b(x)] = x - AG_b(x) \qquad (C19)$$

Eq.(C19) differs slightly from the usual conditions for the a_k's. For very low Reynolds numbers, this difference is significant and hence (C19) is used in the KGS and SW codes.

Appendix D: Lateral-Wall Boundary Layer Relations

From Eqs.(29-32), the boundary layer equations near the lateral wall ($r = 1$) can easily be written. The subscript "$b\ell$" will denote lateral wall boundary layer functions.

$$\frac{\partial(r\underline{u}_{b\ell})}{\partial r} = i\underline{v} - r\frac{\partial \underline{w}_{b\ell}}{\partial x} \qquad (D1)$$

$$\frac{\partial \underline{p}_{b\ell}}{\partial r} = -2\underline{v}_{b\ell} \qquad (D2)$$

$$i(f-1)\underline{v}_{b\ell} = \frac{1}{Re}\frac{\partial^2 \underline{v}_{b\ell}}{\partial r^2} \qquad (D3)$$

$$i(f-1)\underline{w}_{b\ell} = \frac{1}{Re}\frac{\partial^2 \underline{w}_{b\ell}}{\partial r^2} \qquad (D4)$$

The solution of Eqs.(D3-D4) can be written in the form

$$\underline{v}_{b\ell} = v_1(x)exp[(r-1)/\delta_a] + v_0(x)exp[(r_0-r)/\delta_a] \qquad (D5)$$

$$\underline{w}_{b\ell} = w_1(x)exp[(r-1)/\delta_a] + w_0(x)exp[(r_0-r)/\delta_a] \qquad (D6)$$

The no-slip condition at $r = 1$ yields

$$\underline{v}(1,x) = \hat{\underline{v}}(1,x) + v_1 + e_1 v_0 = -(1-f)x \qquad (D7)$$

$$\underline{w}(1,x) = \hat{\underline{w}}(1,x) + w_1 + e_1 w_0 = i(1-f) \qquad (D8)$$

where

$$e_1 = exp[(r_0-1)/\delta_a]$$

$$\hat{\underline{v}} = \hat{v} + \underline{v}_{bc}$$

$$\hat{\underline{w}} = \hat{w} + \underline{w}_{bc}$$

For the partial-fill case, no shear at the free surface yields

$$e_1 v_1 - v_0 = 0 \qquad (D9)$$

$$e_1 w_1 - w_0 = 0 \qquad (D10)$$

Thus

$$v_1 = \frac{-(1-f)x - \hat{\underline{v}}(1,x)}{1+e_1^2}; \quad v_0 = e_1 v_1 \qquad (D11)$$

$$w_1 = \frac{i(1-f) - \hat{\underline{w}}(1,x)}{1+e_1^2}; \quad w_0 = e_1 w_1 \qquad (D12)$$

For a central rod,

$$\hat{\underline{v}}(r_0,x) + e_1 v_1 + v_0 = -(1-f)x \qquad (D13)$$

$$\hat{\underline{w}}(r_0,x) + e_1 w_1 + w_0 = i(1-f)r_0 \qquad (D14)$$

Thus

$$v_1 = \frac{-(1-f)x - \underline{\hat{v}}(1,x)}{1+e_1} - \frac{e_1[\underline{\hat{v}}(1,x) - \underline{\hat{v}}(r_0,x)]}{1-e_1^2} \qquad (D15)$$

$$v_0 = \frac{-(1-f)x - \underline{\hat{v}}(r_0,x)}{1+e_1} + \frac{e_1[\underline{\hat{v}}(1,x) - \underline{\hat{v}}(r_0,x)]}{1-e_1^2} \qquad (D16)$$

$$w_1 = \frac{i(1-f) - \underline{\hat{w}}(1,x)}{1+e_1} - \frac{e_1[\underline{\hat{w}}(1,x) - \underline{\hat{w}}(r_0,x)]}{1-e_1^2} \qquad (D17)$$

$$w_0 = \frac{i(1-f)r_0 - \underline{\hat{w}}(r_0,x)}{1+e_1} + \frac{e_1[\underline{\hat{w}}(1,x) - \underline{\hat{w}}(r_0,x)]}{1-e_1^2} \qquad (D18)$$

The continuity equation can now be used to obtain a relation for u_M.

$$r\underline{u}_M(r,x) = \delta_a\{u_1 exp[(r-1)/\delta_a] - u_0 exp[(r_0-r)/\delta_a]\} \qquad (D19)$$

where

$$\delta_a = (1+i)[2(1-f)Re]^{-1/2}$$

$$u_1 = iv_1 - w_1' \qquad (D20)$$

$$u_0 = iv_0 - r_0 w_0' \qquad (D21)$$

For a partial fill,

$$u_1 = \frac{u_a}{1+e_1^2} \qquad (D22)$$

$$u_0 = e_1 u_1 \qquad (D23)$$

where

$$u_a = -i(1-f)x - \left[\frac{\partial(r\underline{\hat{u}})}{\partial r}\right]_{r=1}$$

For a central rod,

$$u_1 = \frac{u_a}{1+e_1} - \frac{e_1\Delta^*}{1-e_1^2} \qquad (D24)$$

$$u_0 = \frac{u_b}{1+e_1} + \frac{e_1\Delta^*}{1-e_1^2} \qquad (D25)$$

where

$$\Delta^* = \left[\frac{\partial(r\underline{\hat{u}})}{\partial r}\right]_{r=1} - \left[\frac{\partial(r\underline{\hat{u}})}{\partial r}\right]_{r=r_0}$$

$$u_b = -i(1-f)x - \left[\frac{\partial(r\underline{\hat{u}})}{\partial r}\right]_{r=r_0}$$

Thus

$$u_{bl}(1,x) = \left(\frac{1-e_1^2}{1+e_1^2}\right) u_a \qquad \textit{partial fill} \qquad (D26a)$$

$$= \left(\frac{1-e_1}{1+e_1}\right) u_a - \left(\frac{2e_1}{1-e_1^2}\right) \Delta^* \qquad \textit{rod} \qquad (D26b)$$

$$u_{bl}(r_0,x) = 0 \qquad \textit{partial fill} \qquad (D27a)$$

$$= \left(\frac{1-e_1}{1+e_1}\right) u_b + \left(\frac{2e_1}{1-e_1^2}\right) \Delta^* \qquad \textit{rod} \qquad (D27b)$$

The Δ^* terms in the rod expressions above are usually much smaller in magnitude than the other terms and will be neglected.

The boundary condition at r = 1 can be written as

$$\hat{u}(1,x) + \underline{u_{bc}}(1,x) + \underline{u_{bl}}(1,x) = -i(1-f)x \qquad (D28)$$

or

$$\hat{u}(1,x) - \left(\frac{\delta_a e_2}{1-\delta_a e_2}\right) \left[\frac{\partial \hat{u}(r,x)}{\partial r}\right]_{r=1} = -i(1-f)x - \underline{u_{bc}}(1,x) \qquad (D29)$$

where

$$e_2 = \frac{1-e_1^n}{1+e_1^n}, \quad n = 1 \textit{ for a central rod; } 2 \textit{ otherwise}$$

The boundary condition at the rod surface ($r = r_0$) is similar to (D29):

$$\hat{u}(r_0,x) + \left(\frac{\delta_a r_0 e_2}{r_0+\delta_a e_2}\right) \left[\frac{\partial \hat{u}(r,x)}{\partial r}\right]_{r=r_0} = -i(1-f)x - \underline{u_{bc}}(r_0,x) \qquad (D30)$$

INTENTIONALLY LEFT BLANK.

List of Symbols

a	radius of the liquid-payload cylinder
a_k	coefficients in a least-squares fit of x to a sine series ($a_k = 0$ for k = 0,2,4,...)
$\hat{a}_k, \hat{b}_k$	coefficients in the definitions of Z_{1kB} and Z_{6kb}, Eqs.(122-123)
A	c/a, fineness (aspect) ratio of the cylinder
b	radius of the inner cylindrical free surface in a partially-filled cylinder
B	$r^{-2} + \lambda_k^2 - i(1-f)Re$ [replace Re by $q_{2r}Re$ for the two-liquid case]
B_1	$[1-(1-q_1)r_1^4 - q_1 r_0^4]/4$
B_2	$[1-(1-q_3)r_1^2 - q_3 r_0^2]/2$
B_3	$[1-(1-q_1)r_1^2 - q_1 r_c^2]/2$
c	half-height of the liquid-payload cylinder
c_0	$\hat{f}$ for HSG or HSGB; = 0 otherwise
c_k	constant multipliers in the definitions of Z_{nk}, Eqs.(46-51); Fourier coefficients chosen to satisfy boundary conditions
$c_{mpe}, c_{mpl}, c_{mpr}$	that part of $C_{LSM} + iC_{LIM}$ due to the *pressure* on the end-walls, lateral wall, and rod, respectively
$c_{mve}, c_{mvl}, c_{mvr}$	that part of $C_{LSM} + iC_{LIM}$ due to the *viscous stress* on the end-walls, lateral wall, and rod, respectively
CFD	Computational Fluid Dynamics
$C_{LSM} + iC_{LIM}$	$(M_{ye} + iM_{xe})/m_L a^2 \dot{\phi}^2 \tau K$, the liquid side moment and in-plane moment coefficients
C_{LRM}	$M_{ze}/m_L a^2 \dot{\phi}^2 \tau K^2$, the liquid roll moment coefficient
C_p	pressure coefficient, Eq.(150)
d	radius of a central rod within the cylinder

D_k	$\int_{-A}^{A} xG_k(x)dx$
e	$(R/R_0)^{1/2}$, error measure of the fit to Eqs.(101-103)
$\hat{e}_x, \hat{e}_r, \hat{e}_\theta$	unit vectors in the earth-fixed cylindrical system
$\hat{e}_x, \hat{e}_y, \hat{e}_z$	unit vectors in the earth-fixed rectangular system
$\hat{e}_{xc}, \hat{e}_{yc}, \hat{e}_{zc}$	unit vectors in the coning aeroballistic system
e_1	$exp[(r_0 - 1)/\delta_a]$
e_2	$(1 - e_1^n)/(1 + e_1^n)$ where n = 1 for a central rod; otherwise, n = 2
e_3	$exp[(r_1 - 1)/\delta_a]$
e_4	$q_2^{1/2}[1 + q_5 + (1 - q_5)e_3^2] - (1 - q_1)(1 + e_3^2)\delta_a$
e_5	$[1 + q_5 - (1 - q_5)e_3^2]/[1 + q_5 + (1 - q_5)e_3^2]$
e_6	$[1 + q_5 + (1 - q_5)e_3^2][1 - e_5\delta_a]$
f	$(1 - ie)r$
$\hat{f}$	$-2i(1 - f)/(1 + f)$
f_b	$[(3 - f)(1 + f)]^{1/2}/(1 - f)$
g_k	$G_k(A)$, see Eqs.(101-102)
G_k	functions of x in the expressions for $\underline{u}, \underline{v}$, and $\underline{p}$, Eqs.(34-36); $G_0 = x$
h	distance from the projectile center of mass to the cylinder center of mass (positive if the projectile c.m. if forward of the cylinder c.m.)
h_k	$H_k(A)$, see Eq.(103)
H_k	functions of x in the expression for $\underline{w}$, Eq.(33); $H_0 = 1$
HSG	Hall-Sedney-Gerber method, Ref. [2]
HSGB	HSG Binary method

I_k	$\int_{r_0}^{1} q_{1r} Z_{4k}(r) r^2 \, dr$
J_0, J_1	complex Bessel functions of the first kind, order 0 and 1 (with argument $f_b \lambda_k r$)
k	summation index for the perturbation variables, Eqs.(33-36), k = 0,1,2,..., N
K	$\sin \alpha_t$
KGS	Kitchens-Gerber-Sedney method, Ref. [10]
KGSB	KGS Binary method
K^*	$K e^{-i\psi} = K_0 e^{i(f\phi - \theta)}$
K_0	the value of K at $\epsilon\tau\phi = 0$; $K = K_0 e^{\epsilon\tau\phi}$
L	h/a
$\vec{L}$	angular momentum of the liquid
m_L	$2\pi a^2 c \rho_L$
$\vec{M}$	liquid moment
M_{xc}, M_{yc}, M_{zc}	components of the liquid moment in the coning system
p	liquid pressure
p_0	value of p at $r = 0$, $K = 0$
$\underline{p}(r, z)$	complex pressure perturbation, nondimensionalized by $\rho_L a^2 \dot{\phi}^2$
q_1	ρ_2/ρ_1
q_2	ν_1/ν_2
q_3	$\mu_2/\mu_1 = q_1/q_2$
q_4	1 for the partial fill case; 0 otherwise
q_5	$q_1/q_2^{1/2}$

q_{1r}	q_1 (for $r_0 \leq r \leq r_1$) or 1 (for $r_1 < r$)
q_{2r}	q_2 (for $r_0 \leq r \leq r_1$) or 1 (for $r_1 < r$)
q_{3r}	q_3 (for $r_0 \leq r \leq r_1$) or 1 (for $r_1 < r$)
$r, \bar{r}$	earth-fixed and coning radial coordinates, respectively, nondimensionalized by the radius a
r_c	earth-fixed radial coordinate of the cylindrical wall, nondimensionalized by a
$r_f, \bar{r}_f$	earth-fixed and coning radial coordinates of the free surface in a partially-filled cylinder, nondimensionalized by a
$r_i, \bar{r}_i$	earth-fixed and coning radial coordinates of the two-liquid interface (for small-amplitude coning motion), nondimensionalized by a
$r_r, \bar{r}_r$	earth-fixed and coning radial coordinates of the rod, nondimensionalized by a
r_0	(a) for a fully-filled cylinder, 0 (b) for a partially-filled cylinder, the radius b/a of the inner cylindrical surface (for no coning motion) (c) for a cylinder with a central rod, the rod radius nondimensionalized by a
r_1	earth-fixed radial coordinate of the two-liquid interface (for no coning motion), nondimensionalized by a
(r_1^-)	inner-liquid value at r_1
(r_1^+)	outer-liquid value at r_1
R	function minimized in the determination of the c_k's, Eq.(104)
$\vec{R}$	position vector
$R\{\ \}$	real part of a complex quantity
Re	Reynolds number, $a^2\dot{\phi}/\nu$ (or, for two liquids, $a^2\dot{\phi}/\nu_1$, the outer-liquid Reynolds number)
Re_e	Re for $\nu = \nu_e$

R_0	value of R for $c_k = 0$
R_1, R_2, R_3	functions used in determining the c_k's, Eqs.(101-103)
S	Stewartson inviscid method
SB	Stewartson Binary inviscid method
SW	Stewartson-Wedemeyer high-Re method
SWB	Stewartson-Wedemeyer Binary high-Re method
$\underline{u}(r,x)$	complex radial velocity perturbation, nondimensionalized by $a\dot{\phi}$
$\underline{v}(r,x)$	complex azimuthal velocity perturbation, nondimensionalized by $a\dot{\phi}$
$\vec{V}$	velocity vector
V_x, V_r, V_θ	velocity components in the earth-fixed cylindrical system
$\underline{w}(r,x)$	complex axial velocity perturbation, nondimensionalized by $a\dot{\phi}$
$x, \tilde{x}$	earth-fixed and coning axial coordinates, respectively, nondimensionalized by the radius a
X	axis along the projectile's axis of symmetry
X_e, Y_e, Z_e	axes in the earth-fixed system, X_e initially along the velocity vector, Z_e downward
Y_0, Y_1	complex Bessel functions of the second kind, order 0 and 1 (with argument $m\lambda_k r$
Z_{nk}	complex perturbation variables formed from $(\hat{w}_k, \hat{u}_k, \hat{v}_k, \hat{p}_k, \hat{w}'_k, \hat{v}'_k)$, Eqs.(46-51)
α	$(1-i)\sqrt{(3-f)Re/2} = -i\beta\sqrt{(3-f)/(1+f)}$
α_t	total angle of attack; the angle between the X and X_e axes

β	$(1+i)\sqrt{(1+f)Re/2}$
γ	$\cos\alpha_t$
δ_a	$\frac{1+i}{\sqrt{2(1-f)Re}}$
δ_b	$\delta_a q_2^{-1/2}$
δ_c	$\frac{-(1+i)}{2(1-f)\sqrt{2Re}}\left[\frac{1+f}{\sqrt{3-f}}+\frac{i(3-f)}{\sqrt{1+f}}\right]$
δ_{ca}	δ_c for $Re = Re_a$
ΔZ_{nkB}	$Z_{nkB}(r_1^+) - Z_{nkB}(r_1^-)$, the jump in Z_{nkB} at the two-liquid interface
ϵ	(yaw damping rate)/(coning rate) $= (\dot{K}/K)/(\dot{\phi}_a)$
θ	earth-fixed azimuthal coordinate
λ_k	complex eigenfrequencies arising in the expressions for the perturbation variables, Eqs.(33-36), where $\lambda_0 = 0$
λ_{k1}	0 (if k = 0), λ_k (if $k > 0$)
λ_{k2}	1 (if k = 0), λ_k (if $k > 0$)
μ_1, μ_2	outer- and inner-liquid dynamic viscosities, respectively ($\mu_j = \nu_j \rho_j$)
ν	kinematic viscosity of the liquid
ν_a	average two-liquid value of the kinematic viscosity, Eq.(126)
ν_1, ν_2	outer- and inner-liquid kinematic viscosities, respectively
ρ_L	density of the liquid (or, for two liquids, the density ρ_1 of the outer liquid)
ρ_1, ρ_2	outer- and inner-liquid densities, respectively
τ	$\dot{\phi}_a/\dot{\phi}$
φ	$\dot{\phi}t$, the roll angle
$\dot{\phi}$	spin rate (assumed positive and constant); the axial component

	of the projectile's angular velocity with respect to an *inertial* frame
ϕ_α	the angle between the Z_e-axis and the normal to the $X - X_e$ plane
$\dot{\phi}_\alpha$	precessional rate of the angular motion performed by the projectile about the velocity vector
ψ	$\theta - \phi_\alpha = \theta - \tau\phi$
$\tilde{\psi}$	coning system azimuthal coordinate
$\vec{\Omega}$	angular velocity of the coning aeroballistic system

Misc.:

$\dot{(\,)}$	$d(\,)/dt$
$(\,)'$	$d(\,)/dr$

INTENTIONALLY LEFT BLANK.

No of Copies	Organization
(Unclass, unlimited) 12	Administrator
(Unclass, limited) 2	Defense Technical Info Center
(Classified) 2	ATTN: DTIC-DDA
	Cameron Station
	Alexandria, VA 22304-6145
1	HQDA (SARD-TR)
	WASH DC 20310-0001
1	Commander
	US Army Materiel Command
	ATTN: AMCDRA-ST
	5001 Eisenhower Avenue
	Alexandria, VA 22333-0001
1	Commander
	US Army Laboratory Command
	ATTN: AMSLC-DL
	Adelphi, MD 20783-1145
2	Commander
	Armament RD&E Center
	US Army AMCCOM
	ATTN: SMCAR-MSI
	Picatinny Arsenal, NJ 07806-5000
2	Commander
	Armament RD&E Center
	US Army AMCCOM
	ATTN: SMCAR-TDC
	Picatinny Arsenal, NJ 07806-5000
1	Director
	Benet Weapons Laboratory
	Armament RD&E Center
	US Army AMCCOM
	ATTN: SMCAR-LCB-TL
	Watervliet, NY 12189-4050
1	Commander
	US Army Armament, Munitions and Chemical Command
	ATTN: SMCAR-ESP-L
	Rock Island, IL 61299-5000
1	Commander
	US Army Aviation Systems Command
	ATTN: AMSAV-DACL
	4300 Goodfellow Blvd.
	St. Louis, MO 63120-1798
1	Director
	US Army Aviation Research and Technology Activity
	Ames Research Center
	Moffett Field, CA 94035-1099

No of Copies	Organization
1	Commander
	US Army Missile Command
	ATTN: AMSMI-RD-CS-R (DOC)
	Redstone Arsenal, AL 35898-5010
1	Commander
	US Army Tank Automotive Command
	ATTN: AMSTA-TSL (Technical Library)
	Warren, MI 48397-5000
1	Director
	US Army TRADOC Analysis Command
	ATTN: ATAA-SL
	White Sands Missile Range, NM 88002-5502
(Class. only) 1	Commandant
	US Army Infantry School
	ATTN: ATSH-CD (Security Mgr.)
	Fort Benning, GA 31905-5660
(Unclass. only) 1	Commandant
	US Army Infantry School
	ATTN: ATSH-CD-CSO-OR
	Fort Benning, GA 31905-5660
(Class. only) 1	The Rand Corporation
	P.O. Box 2138
	Santa Monica, CA 90401-2138
1	Air Force Armament Laboratory
	ATTN: AFATL/DLODL
	Eglin AFB, FL 32542-5000

Aberdeen Proving Ground

Dir, USAMSAA
ATTN: AMXSY-D
AMXSY-MP, H. Cohen

Cdr, USATECOM
ATTN: AMSTE-TO-F

Cdr, CRDEC, AMCCOM
ATTN: SMCCR-RSP-A
SMCCR-MU
SMCCR-MSI

Dir, VLAMO
ATTN: AMSLC-VL-D

No. of Copies	Organization
5	Commander Armament RD&E Center US Army AMCCOM ATTN: SMCAR-LCA-F Mr. D. Mertz Mr. E. Falkowski Mr. R. Kline Mr. S. Kahn Mr. S. Wasserman Picatinny Arsenal, NJ 07806-5000
2	Commander US Army Research Office ATTN: Dr. R.E. Singleton Dr. Jagdish Chandra P.O. Box 12211 Research Triangle Park, NC 27709-2211
1	AGARD-NATO ATTN: R.H. Korkegi APO New York, 09777
10	Central Intelligence Agency Office of Central Reference Dissemination Branch Room GE-47 HQS Washington, DC 20505
3	Commander Naval Air Systems Command ATTN: AIR-604 Washington, DC 20360
1	Commander Naval Surface Weapons Center ATTN: DX-21, Library Branch Dahlgren, VA 22448
2	Commander David W. Taylor Naval Ship Research and Development Command ATTN: H.J. Lugt, Code 1802 S. de los Santos Bethesda, MD 20084
3	Commander Naval Surface Weapons Center Applied Aerodynamics Division ATTN: M. Ciment A.E. Winkelmann W.C. Ragsdale Silver Spring, MD 20910
1	Director Office of Naval Research ATTN: Richard Whiting, Code 123 800 Quincy Street Arlington, VA 22217
2	AFWAL ATTN: J.S. Shang W.L. Hankey Wright-Patterson AFB, OH 45433
1	Aerospace Corporation Aero-Engineering Subdivision ATTN: Walter F. Reddall El Segundo, CA 90245
5	Director National Aeronautics and Space Administration ATTN: D.R. Chapman W.C. Rose B. Wick P. Kutler Technical Library Ames Research Center Moffett Field, CA 94035
4	Director National Aeronautics and Space Administration Langley Research Center ATTN: E. Price J. South J.R. Sterrett Technical Library Langley Station Hampton, VA 23365
1	Director National Aeronautics and Space Administration Lewis Research Center ATTN: MS 60-3, Technical Library 21000 Brookpark Road Cleveland, OH 44135-3127
1	AVCO Corporation Textron Defense Systems Division ATTN: B. Reeves 201 Lowell Street Wilmington, MA 01887

No. of Copies	Organization
2	Director National Aeronautics and Space Administration Marshall Space Flight Center ATTN: A.R. Felix, Chief, S&E-AERO-AE Dr. W.W. Fowlis Huntsville, AL 35812
3	Aerospace Corporation ATTN: H. Mirels R.L. Varwig Aerophysics Laboratory P.O. Box 92957 Los Angeles, CA 90009
2	Director Jet Propulsion Laboratory ATTN: L.M. Mach Technical Library 4800 Oak Grove Drive Pasadena, CA 91103
3	Arnold Research Organization Inc. ATTN: J.D. Whitfield R.K. Matthews J.C. Adams Arnold AFB, TN 37389
3	Boeing Commercial Airplane Company ATTN: R.A. Day, MS 1W-82 P.E. Rubbert, MS 3N-19 J.D. McLean, MS-3N-19 Seattle, WA 98124
1	Calspan Corporation ATTN: A. Ritter P.O. Box 400 Buffalo, NY 14225
2	Lockheed-Georgia Company ATTN: B.H. Little, Jr. G.A. Pounds Department 72074, Zone 403 86 South Cobb Drive Marietta, GA 30062
1	General Dynamics ATTN: Research Library 2246 P.O. Box 748 Fort Worth, TX 76101
1	General Electric Company, RESD ATTN: W.J. East 3198 Chestnut Street Philadelphia, PA 19101
2	Grumman Aerospace Corporation ATTN: R.E. Melnik L.G. Kaufman Bethpage, NY 11714
1	Lockheed Missiles and Space Company ATTN: Technical Information Center 3251 Hanover Street Palo Alto, CA 94304
3	Martin-Marietta Corporation ATTN: S.H. Maslen S.C. Traugott H. Obremski 1450 S. Rolling Road Baltimore, MD 21227
2	McDonnell Douglas Astronautics Corporation ATTN: J. Xerikos H. Tang 5301 Bolsa Avenue Huntington Beach, CA 92647
1	Douglas Aircraft Company ATTN: T. Cebeci 3855 Lakewood Boulevard Long Beach, CA 90846
3	Rockwell International Science Center ATTN: Dr. V. Shankar Dr. S. Chakravarthy Dr. N. Malmuth 1049 Camino Dos Rios Thousand Oaks, CA 91360
4	Sandia National Laboratory ATTN: G. Wolfe W.L. Oberkampf F.G. Blottner G.F. Homicz Albuquerque, NM 87185
2	United Aircraft Corporation Research Laboratory ATTN: M.J. Werle Library East Hartford, CT 06108

No. of Copies	Organization
1	LTV Aerospace and Defense Company Vought Missiles and Advanced Programs Division P.O. Box 650003 Dallas, TX 75265-0003
2	Arizona State University Department of Mechanical and Energy Systems Engineering ATTN: G.P. Neitzel W.S. Saric Tempe, AZ 85287
1	Cornell University Graduate School of Aerospace Engineering ATTN: Library Ithaca, NY 14853
3	California Institute of Technology ATTN: Technical Library H.B. Keller, Math Department D. Coles, Aerospace Department Pasadena, CA 91109
1	Director The Johns Hopkins University Applied Physics Laboratory Johns Hopkins Road Laurel, MD 20707
1	California Institute of Technology Jet Propulsion Laboratory ATTN: Dr. Guy K. Man 4800 Oak Grove Drive Pasadena, CA 91109
2	Illinois Institute of Technology ATTN: S. Rosenblat H.M. Nagib 3300 South Federal Chicago, IL 60616
1	Southwest Research Institute Department of Mechanical Sciences ATTN: Franklin T. Dodge San Antonio, TX 78284
1	Vought Corporation ATTN: J.M. Cooksey, Chief Gas Dynamics Laboratory, 2-53700 P.O. Box 5907 Dallas, TX 75222

No. of Copies	Organization
1	Louisiana State University Department of Physics and Astronomy ATTN: Dr. R.G. Hussey Baton Rouge, LA 70803
3	Massachusetts Institute of Technology ATTN: E. Covert H. Greenspan Technical Library 77 Massachusetts Avenue Cambridge, MA 02139
2	North Carolina State University Mechanical and Aerospace Engineering Department ATTN: F.F. DeJarnette J.C. Williams Raleigh, NC 27607
1	Notre Dame University Department of Aerospace Engineering ATTN: T.J. Mueller South Bend, IN 46556
1	Northwestern University Department of Engineering Science and Applied Mathematics ATTN: Dr. S.H. Davis Evanston, IL 60201
2	The Ohio State University Department of Aeronautical Engineering and Astronautical Engineering ATTN: S.L. Petrie O.R. Burggraf Columbus, OH 43210
1	The Ohio State University Department of Mechanical Engineering ATTN: Dr. T. Herbert 206 W. 18th Avenue Columbus, OH 43210-1107
2	Polytechnic Institute of New York ATTN: G. Moretti Technical Library Route 110 Farmingdale, NY 11735
1	Purdue University Thermal Science and Propulsion Center ATTN: Technical Library W. Lafayette, IN 47906

No. of Copies	Organization
3	Princeton University James Forrestal Research Center Gas Dynamics Laboratory ATTN: S.M. Bogdonoff S.I. Cheng Technical Library Princeton, NJ 08540
1	Rensselaer Polytechnic Institute Department of Math Sciences ATTN: Technical Library Troy, NY 12181
1	Rutgers University Department of Mechanical, Industrial, and Aerospace Engineering ATTN: R.H. Page New Brunswick, NJ 08903
1	Southern Methodist University Department of Civil and Mechanical Engineering ATTN: R.L. Simpson Dallas, TX 75272
1	Southwest Research Institute Applied Mechanics Reviews 8500 Culebra Road San Antonio, TX 78228
1	San Diego State University Department of Aerospace Engineering and Engineering Mechanics College of Engineering ATTN: K.C. Wang San Diego, CA 92115
1	Harvard University Division of Engineering and Applied Physics ATTN: G.J. Carrier Cambridge, MA 01238
1	Texas A&M University College of Engineering ATTN: R.H. Page College Station, TX 77843
1	Stanford University Department of Aeronautics/Astronautics ATTN: M. VanDyke Stanford, CA 94305

No. of Copies	Organization
1	University of California - Davis ATTN: H.A. Dwyer Davis, CA 95616
1	University of California - Berkeley Department of Aerospace Engineering ATTN: M. Holt Berkeley, CA 94720
1	University of California - San Diego Department of Aerospace Engineering and Mechanical Engineer Sciences La Jolla, CA 92307
1	University of Santa Clara Department of Physics ATTN: R. Greeley Santa Clara, CA 95053
2	University of Cincinnati Department of Aerospace Engineering ATTN: R.T. Davis S.G. Rubin Cincinnati, OH 45221
1	University of Colorado Department of Astro-Geophysics ATTN: E.R. Benton Boulder, CO 80302
2	University of Maryland ATTN: W. Melnik J.D. Anderson College Park, MD 20740
1	University of Maryland - Baltimore County Department of Mathematics ATTN: Dr. Y.M. Lynn 5401 Wilkens Avenue Baltimore, MD 21228
1	University of Texas Department of Aerospace Engineering ATTN: J.C. Westkaemper Austin, TX 78712
2	University of Southern California Department of Aerospace Engineering ATTN: T. Maxworthy P. Weidman Los Angeles, CA 90007

No. of Copies	Organization
2	University of Michigan Department of Aeronautical Engineering ATTN: W.W. Wilmarth Technical Library East Engineering Building Ann Arbor, MI 48104
2	University of Rochester Department of Mechanical and Aerospace Sciences ATTN: R. Gans A. Clark, Jr. Rochester, NY 14627
1	University of Virginia Department of Aerospace Engineering and Engineering Physics ATTN: I.D. Jacobson Charlottesville, VA 22904
1	University of California - Santa Barbara Department of Mechanical and Environmental Engineering ATTN: J.P. Vanyo Santa Barbara, CA 93106
4	University of Virginia Department of Mechanical and Aerospace Engineering ATTN: W.G. Wood R.J. Ribando R. Krauss W.E. Scott Charlottesville, VA 22904
1	University of Tennessee Department of Physics ATTN: Technical Library Knoxville, TN 37916
1	University of Washington Department of Mechanical Engineering ATTN: Technical Library Seattle, WA 98105
1	University of Wyoming ATTN: D.L. Boyer University Station Laramie, WY 82701

No. of Copies	Organization
1	University of Wisconsin - Madison Center for Mathematical Sciences ATTN: John C. Strikwerda 610 Walnut Street Madison, WI 53705
1	Woods Hole Oceanographic Institute ATTN: J.A. Whitehead Woods Hole, MA 02543
2	Virginia Polytechnic Institute and State University Department of Aerospace Engineering ATTN: Technical Library Dr. T. Herbert Blacksburg, VA 24061
1	ICASE ATTN: Professor Philip Hall Mail Stop 132C NASA Langley Research Center Hampton, VA 23665

ABERDEEN PROVING GROUND

2	Cdr, CRDEC AMCCOM ATTN: SMCCR-RSP-A (Mr. Miles Miller) (Mr. Daniel Weber)

USER EVALUATION SHEET/CHANGE OF ADDRESS

This Laboratory undertakes a continuing effort to improve the quality of the reports it publishes. Your comments/answers to the items/questions below will aid us in our efforts.

1. BRL Report Number TR-3074 Date of Report DEC 89

2. Date Report Received _____

3. Does this report satisfy a need? (Comment on purpose, related project, or other area of interest for which the report will be used.) _____

4. How specifically, is the report being used? (Information source, design data, procedure, source of ideas, etc.) _____

5. Has the information in this report led to any quantitative savings as far as man-hours or dollars saved, operating costs avoided or efficiencies achieved, etc? If so, please elaborate. _____

6. General Comments. What do you think should be changed to improve future reports? (Indicate changes to organization, technical content, format, etc.)

_____

_____

_____

CURRENT ADDRESS

_____
Name

_____
Organization

_____
Address

_____
City, State, Zip

7 If indicating a Change of Address or Address Correction, please provide the New or Correct Address in Block 6 above and the Old or Incorrect address below.

OLD ADDRESS

_____
Name

_____
Organization

_____
Address

_____
City, State, Zip

(Remove this sheet, fold as indicated, staple or tape closed, and mail.)

FOLD HERE

Director
U.S. Army Ballistic Research Laboratory
ATTN: SLCBR-DD-T
Aberdeen Proving Ground, MD 21005-5066

OFFICIAL BUSINESS

NO POSTAGE
NECESSARY
IF MAILED
IN THE
UNITED STATES

BUSINESS REPLY MAIL
FIRST CLASS PERMIT NO 12062 WASHINGTON, DC

POSTAGE WILL BE PAID BY DEPARTMENT OF THE ARMY

Director
U.S. Army Ballistic Research Laboratory
ATTN: SLCBR-DD-T
Aberdeen Proving Ground, MD 21005-9989

FOLD HERE